An Improved Shashlyk Calorimeter

G.S. Atoian [a,c], G.I. Britvich [b], S.K. Chernichenko [b], S. Dhawan [c], V.V. Issakov [a,c], O.V. Karavichev [a], T.L. Karavicheva [a], V.N. Marin [a], A.A. Poblaguev [a,c,*], I.V. Shein [b], A.P. Soldatov [b], and M.E. Zeller [c]

[a] *Institute for Nuclear Research of Russian Academy of Sciences, Moscow 117312, Russia*

[b] *Institute for High Energy Physics, Protvino 142284, Russia*

[c] *Physics Department, Yale University, New Haven, CT 06511, USA*

Abstract

Shashlyk electromagnetic calorimeter modules with an energy resolution of $3\%/\sqrt{E\ (\mathrm{GeV})}$ for $100 \div 1000$ MeV photons has been developed, and a prototype tested. Details of these improved modules, including mechanical construction, selection of wave shifting fibers and of the photodetector, and developement of a new scintillator with improved optical and mechanical properties appropriate for use in the modules are described. How the modules will perform in a large calorimeter was determined from prototype measurements. The experimentally determined characteristics for the calorimeter prototype show energy resolution of $\sigma_E/E = (1.96 \pm 0.1)\% \oplus (2.74 \pm 0.05)\%/\sqrt{E\ (\mathrm{GeV})}$, time resolution of $\sigma_T = (90 \pm 10)$ psec$/\sqrt{E\ (\mathrm{GeV})}$, and a photon detection inefficiency due to fiber holes of $\epsilon \leq 5 \times 10^{-5}$ $(\Theta_{\mathrm{beam}} > 5$ mrad).

Key words: Shashlyk calorimeter, Monte-Carlo simulation, APD, WLS fiber, scintillator
PACS: 29.40.Vj, 07.05.Tp

1 Introduction.

The Shashlyk technique for electromagnetic colorimetry [1] has been in use for several years. In designing a large calorimeter for the KOPIO experiment [2] we have devloped an improved Shashlyk module for such a device. This

* Corresponding author. *E-mail address:* poblaguev@bnl.gov (A.A. Poblaguev)

paper describes the design and construction of the module, as well as the unit's performance in prototype tests. It is further development of the work described in Ref [3].

The requirements of the KOPIO experiment led to the following specifications:

- Energy range: $50 \div 1000$ MeV.
- Energy resolution: $\approx 3.0\%/\sqrt{E(\mathrm{GeV})}$.
- Time resolution: ≈ 100 psec $/\sqrt{E\ (\mathrm{GeV})}$.
- Photon detection inefficiency: $\leq 10^{-4}$.
- Granularity: ~ 10 cm.
- Size of the Calorimeter: 4.4×4.4 m^2.
- Operation in a magnetic field of up to 500 Gauss.

The Shashlyk approach, in which modules are constructed of lead-scintillator sandwiches read out by means of Wavelength-Shifting (WLS) fibers passing through holes in the scintillator and lead [1], is appropriate for such specifications since the performance level can be achieved economically with well understood and reliable techniques. While we describe a module with significantly improved performance over previous manifestations, the technique is well proved by us, *e.g.* experiment E865 at Brookhaven [1,4], and has been adopted by others, *e.g.* the PHENIX RHIC detector [5], the HERA-B detector at DESY [6], and the LHCb detector at CERN [7].

2 Approach to improving the Shashlyk module

At the outset of improving the module a detailed simulation model was developed [3]. This model is based on a GEANT3 [8] description of electromagnetic shower and a special optical simulation of the light collection in the scintillator plates. Input for the model was experimental and test beam data. The model output correlated well with data. Analyzing the performance of the prototype Shashlyk module with energy resolution of about $4\%/\sqrt{E(\mathrm{GeV})}$ [1] we found, that energy resolution of about $3.0\%/\sqrt{E(\mathrm{GeV})}$ could be reached after some optimization of the module's mechanical and optical properties (see details in Ref. [3] and [9]).

We revisited the mechanical and optical construction as described below, and optimized the selection of WLS fibers and the photodetector. A new scintillator with improved optical and mechanical properties was specially developed

[1] This module was described in details in Ref. [3]. In this paper we will refer to it as to "standard" Shaslyk module.

at the IHEP scintillator facility (Protvino, Russia) [10]. The corresponding improvements to the module design were implemented in the new KOPIO Calorimeter prototype modules, which were equiped with an Avalanche Photo Diode (APD) and Wave-Form Digitazer (WFD) readout.

2.1 Mechanical construction of the improved Shashlyk module.

The design of the new prototype module is shown in Fig. 1. The module is a sandwich of alternating perforated stamped lead and injection-molded polystyrene-based scintillator plates. The cross sectional size of a module is 110×110 mm^2. There are 300 layers, each layer consisting of a 0.275-mm lead plate and 1.5-mm scintillator plate. The lateral size of a lead or scintillator plate is 109.7×109.7 mm^2. Each plate has 144 holes equidistantly arranged in a 12×12 matrix, the spacing between the holes being 9.3 mm. The diameter of the holes is 1.3 mm, both in the lead and the scintillator plates. Inserted into the holes are 72 WLS fibers, with each fiber looped at the front of the module so that both ends of a fiber are viewed by a photodetector. Such a loop (radius $\sim$2.5 cm) may be approximated by a mirror with a reflection coefficient of about 95% [11]. The fiber ends are collected in one bunch, squeezed, cut and polished, and connected to a photodetector though a small air gap. The complete stack of all plates is held in compression by four 1-mm stainless steel wires. The module is wrapped with 150-μm TYVEK paper which has good light reflection efficiency of about 80%.

The module is assembling into a special assembling berth that allows to subject the assembled modules to cyclic longitudinal loadings up to 800 kg. This procedure prevents a subsequent longitudinal shrinkage of the assembled modules and provides a long-term stabilization of a sensitive length of the module with accuracy of $\simeq 1mm$.

The mechanical parameters of the module are summarized in Table 1.

2.2 Improvements of the Module Geometry

The mechanical construction of the module was revisited to minimize the insensitive area, to increase the effective radiation density, and to improve the sampling ratio and transverse light collection uniformity.

An important innovation in the mechanical design of the module is the "LEGO"-type locks for the scintillator tiles shown in Fig. 1. These locks, four per tile, fix the position of the scintillators with the 350-μm gaps, providing sufficient room for the 275-μm lead tiles without optical contacts between lead and scin-

tillator. The mechanical structure enables removal of 600 paper tiles, which were preventing optical contact between the scintillator and lead in the "standard" Shashlyk design, reducing the diameter of the fiber holes to 1.3 mm, and removal of the compressing steel tapes at the sides of the module. Compared to the "standard" Shashlyk module, the holes/cracks and other insensitive areas were reduced from 2.5% to 1.6%, and the module's mechanical properties such as dimensional tolerances and constructive stiffness were significantly improved. By removing the paper tiles, the effective radiation length could be reduced from 4.0 cm to 3.5 cm.

The sampling, i.e. the relation between thicknesses of lead and scintillator tiles, dominates in the energy resolution of the Shashlyk module. However, there is only a limited ability to improve the "pure" sampling contribution to the energy resolution of the Shashlyk module. Decreasing the thickness of the lead only will increase the length of the module, while the proportional decreasing of both the lead and scintillator thicknesses will reduce the light collection efficiency. Nevertheless, by removing the paper between the lead and scintillator tiles, both the sampling could be improved and the length of the module could be shortened. Compared to the design of the previous module [3], the sampling ratio was improved by a factor of 1.25.

The dominant source of non-uniformity of the light collection is the absorption of light at the edges of a scintillator tile. For improvement, the reflection efficiency on the edges of the scintillator tile is crucial. In the new module, the WLS fiber density was effectively increased by "cutting the edges" of the scintillator tile. The transverse size of the tile, 10.97 cm, is smaller that the "uniform" size of 11.16 cm for 12 fibers with 0.93-cm spacing. In addition, the module was wrapped with TYVEK paper (reflection efficiency about 80%). As a result, the light collection efficiency at the edges of the scintillator tile is only 2.3% smaller than in the center of the tile for the point-like light source. In the case of a 250-MeV photon shower, the difference is only 0.5%, which is negligible compared to the energy resolution of about 6% for such photons.

The experimental results for the light collection uniformity for TYVEK and Xerox copier papers are presented in Fig. 2. The measurements were made with a scintillator tile exposed to collimated ^{90}Sr electrons. For comparison, the simulated light collection efficiencies are shown. One can see that the is good consistency between the optical simulations and measurements. Further improvement may be achieved if Millipore paper with reflection efficiency of 90% will be used [12].

2.3 WLS Fibers

A main concern about the WLS fibers for the Shashlyk readout is the light attenuation length in a fiber. Because the longitudinal fluctuations of electromagnetic showers are about 3-4 cm (one radiation length), the effective attenuation length in fibers must be greater than 3–4 m to have this contribution to the energy resolution be much smaller than the sampling contribution. We have experimentally measured the light attenuation in three different multiclad WLS fibers: (i) BCF-99-29AA, (ii) KURARAY Y11(200)M and (iii) KURARAY Y11(200)MS. Measurements were made by using a collimated light source and muons that penetrated the modules transversely. The size of the beam spot was 1×1 cm^2. Results of the measurements are presented in Fig. 3. It should be noted that the measured values of effective attenuation lengths include the effects of the fiber loop and the short-distance component of light attenuation in the fibers, which have important roles in the light transmission over short distances. The effective attenuation length of 3.6 m in KURARAY Y11(200)MS fiber satisfies our requirements. In comparison with other fibers, this commercial fiber also provides the best reemission efficiency of blue scintillation light, and it has excellent mechanical properties – high tensile and bending strength – and high uniformity in cross-sectional dimensions. For example, its light reemission efficiency is a factor of 1.5 larger than that for any Bicron WLS fiber, and the diameter for any round fiber varies by no more than 2.0%.

2.4 Scintillator

An important contribution for the improvement of the photostatistics over earlier designs of Shashlyk modules is the use of new scintillator tiles with an increased light collection efficiency. An optimization of the light yield of the scintillator tiles for the KOPIO Shashlyk modules has been developed and carried out at the IHEP scintillator facility (Protvino, Russia) [10]. In the previous Shashlyk calorimeters, scintillators based on PSM115 polystyrene was used. The new modules employ BASF143E-based scintillator. The test results for the several scintillators are shown in Table 2.

Though there is no actual increase in the amount of light produced by a charge particle, the light collection efficiency in the scintillator tile has a gain by a factor of 1.6. Because the index of refraction for the polystyrene-based scintillator is 1.59, only light from total internal reflection at the large side of the scintillator tile can be captured by a WLS fiber. The total internal reflection efficiency can potentially be as large as 100%. However, this value is not reachable for realistic surfaces. Many reflections usually occur before light

is captured and re-emitted by a WLS fiber. Both the effective attenuation length and the light collection efficiency in a scintillator tile depends on the light reflection efficiency. As shown in Fig. 4, the parametric dependence of the light collection efficiency on the attenuation length, calculated from our optical model [3], is in a good agreement with the experimental results shown in Table 2.

The new plastic base of the scintillator material and the new production technology of tiles yields a 97% reflection efficiency from the scintillator surface, and strongly improves the reproduction quality (see Fig. 5) of the tiles. The latter is crucial for good longitudinal light collection uniformity. Due to the fluctuation of the depth of the electromagnetic shower in the calorimeter module, good reproduction quality of the tiles is a mandatory condition for an appropriate performance of the $3\%/\sqrt{E\ (\mathrm{GeV})}$ module.

Fluors for the new scintillator composition, BASF143E polystyrene + 1.5%pTP + 0.04%POPOP were selected [13,14] to match well with the absorption spectrum of the Kuraray Y11(200)MS WLS fiber (Fig. 6). With a selected BASF143E-based scintillator and KURARAY fibers, the effective light yield in the KOPIO Shashlyk module (at the entrance to the photodetector) becomes $N_\gamma \sim$60 photons per 1 MeV of the incident photon energy.

The radiation hardness of the scintillator may be a limitation factor for using Shashlyk calorimeter in the modern high statistics experiment. It was reported [13] that the radiation stability of BASF143E-based scintillator is a dose level 120 krad, and the recovery time is about 80 days. This limitation would not be a problem for the KOPIO Calorimeter for which this Shashlyk module was designed.

2.5 Photodetector

The Avalanche Photo Diode, a detector with high quantum efficiency, provides another important improvement of the photostatistics contribution to the energy resolution of the KOPIO Shashlyk module.

Our preliminary experimental studies of the fine-sampling Shashlyk modules [3] have shown that the performance of Shashlyk calorimeter modules with photomultiplier (PMT) readouts agrees with the simulations and nearly satisfies the requirements formulated in the Introduction. However, these test measurements were made in an optimal environment for PMT readout: no magnetic fields, short measuring runs, and continuous and stable photon beams.

These conditions do not properly represent those that would be encountered in the KOPIO experimental environment. Our main concern is related to the

leakage of the magnetic field from the downstream magnet of up to 500 Gauss. Another serious problem is the cycling of real beam every several seconds, with possible significant variations in intensity. This will produce short- and long-term variations of the PMT gain, which will destroy the response stability of the detector performance. In addition, the quantum efficiency of PMTs, which is about 18% at 500 nm (the region of WLS-fiber response) for the best "standard" green-sensitive tubes, is relatively low.

Consideration was thus given to alternative photodetectors. Recent progress in the development of new APD with large active areas (up to 200 mm^2), low capacitance, low dark current, high gain (up to 1,000), and high quantum efficiency (up to 90%) allows us to consider these photodetectors as primary candidates for the improved Shashlyk Calorimeter. Some characteristics of some large-area APDs available in 2003 are shown in Table 3. For comparison, the parameters of the green-sensitive PMT-9903B and the well-known small-area Hamamatsu APD S8664-55 are also displayed. Here, we briefly report the results of our study of the large area APDs.

Operation in magnetic fields: APDs can operate in a magnetic field of up to 80 kG [15].

Size of the active area: The fibers from the Shashlyk module, described in this paper, are collected to a 14 mm diameter bunch. This size is well matched to the Advanced Photonics Inc. APD 630-70-74-510 (API APD), which has diameter of 16 mm.

Response uniformity of the active area: This feature is important for the Shashlyk module because each fiber delivers light to only a small part of the total sensitive area.The response of the selected APD varies by less than 3% over the active area (Fig. 7). Usually, PMTs exhibit poor spatial response uniformity ($\geq 20\%$).

Quantum efficiency of the sensitive area: Photostatistics, directly dependent on the quantum efficiency (Q) of the photodetector, is an important contribution to the energy resolution of a calorimeter. For green light emitted by Kuraray fibers, the APDs have much higher quantum efficiencies than PMTs (see Fig. 8). For example, the quantum efficiency of the API APD is 94%, a factor 5 higher than quantum efficiency of the 9903B PMT. It should be noted that that the photostatistics contribution depends also on the fluctuations of the photodetector gain, $(\sigma_E/E)^2_{\rm ph.stat.} = F/QN_\gamma$, where F is the so-called excess noise factor and N_γ is the number of primary photons at the entrance of the photodetector. For an ideal photodetector, $F = 1$, for a high-linearity PMT $F_{\rm PMT}$ is usually between 1.3 and 1.6. For a high-gain APD, excess noise factor linearly depends on the gain $M_{\rm APD}$, $F_{\rm APD} \simeq 2 + kM_{\rm APD}$ [16,17]. The experimentally measured behavior of $F_{\rm APD}$ versus $M_{\rm APD}$, for some selected

APDs, is shown in Fig. 9. Taking into account both quantum efficiency Q and excess noise factor F, we conclude that API APD has best "photostatistics quality", $Q/F \simeq 43\%$, $(M_{\rm APD} \simeq 100)$, about a factor 3.5 better than 9903B PMT.

Electronic noise of the photodetector/amplifier chain: The contribution of the electronic noise of the photodetector/amplifier chain to the energy resolution is usually referred to as the Equivalent Noise Charge (ENC) of a photodetector readout chain, $\sigma_{\rm ENC}$. In the case of a Charge Sensitive Amplifier (CSA) with a simple *CR-RC* shaper, the ENC can be estimated from:

$$\sigma^2_{\rm ENC} = \frac{I_S/M^2 + I_B F}{4q}\Delta t + \sigma^2_{\rm amp}/M^2, \qquad (1)$$

where q is the charge of an electron, Δt is the charge integrating time of the photodetector/amplifier chain, and $\sigma_{\rm amp}$ is the ENC of the amplifier. The surface leakage current I_S and bulk current I_B are two independent components of the photodetector dark current $I_d = I_S + I_B M$. It is assumed that Δt is larger than the signal pulse duration. For a PMT readout without an amplifier, $\sigma_{\rm ENC} \simeq 0$ due to a very small PMT dark current. The experimentally measured behavior of the APD dark current versus $M_{\rm APD}$ for some selected APDs is shown in Fig. 10. For the API APD, the ENC contributions of the leakage current to the energy resolution can be estimated as $\simeq 14$ electrons for $\Delta t \approx 100$ ns and $M_{\rm APD} \geq 100$. The value of the amplifier noise $\sigma_{\rm amp}$ is usually measured experimentally. The noise characteristics of some fast CSAs are shown in Fig. 11. For the API APD, which has capacitance about 130 pF, and the $2 \times$ SK2394 CSA, the amplifier noise may be estimated as $\sigma_{\rm amp}/M_{\rm APD} \simeq 18$ for $M_{\rm APD} \simeq 100$. Assuming 60 photons at the entrance of photodetector per 1 MeV of the deposited energy, the total electronic noise contribution to the energy resolution of the Shashlyk module is about 0.4 MeV for the API APD. This value is negligible for the assumed photon energy range of $100 \div 1000$ MeV..

Gain and noise dependence on the temperature: The APD performance is very sensitive to the environmental temperature. Because $\frac{1}{M}\frac{dM}{dT} \simeq -4\%$, temperature and gain monitoring is an important condition of using APDs in the experiment. For the API APD, the noise dependence on temperature is shown in Fig. 12. To reduce noise, a thermostable cooling system should be used.

Gain dependence on High Voltage: According to our experimental study of the API APD, $\frac{1}{M}\frac{dM}{dV} \approx (2-3)\%$ depending on the environment temperature and gain. The dependence is similar to those of PMTs.

Gain dependence on the rate: Contrary to PMTs, there is almost no dependence of APD gain on rate. In our test measurements with API APDs, we did

not find any gain variations for the rates up to few MHz. However, APDs are used with preamplifiers. For slow preamplifiers, there may be a rate dependence due to the pile-up.

Time response of the API APD: The time response of the API APD to a short-duration (3 ns) light pulse with an intensity corresponding to 700-MeV photon, is shown in Fig. 13. One can see that a rise time of the APD response pulse (without any amplifier) is fast enough. Its value of 5.9 ns is comparable with 3.7 ns for the PMT-9903B response to the same light pulse. The fall time of the APD response pulse, 18.1 ns, is longer than that for the PMT response, 7.2 ns, due to higher APD capacitance. The difference between PMT and APD time response becomes less essential if we take into account the Shashlyk module signal duration (see Fig. 23).

To summarize, the Advanced Photonics Inc. APD 630-70-74-510 was chosen for the test beam measurements because it has the best properties for photoelectron statistics and for electronic noise. This commercial device has the highest quantum efficiency over a wide spectral range (see Fig. 8), the lowest dark current and, especially, the lowest bulk dark current (see Fig. 10) compared with other pre-selected APDs. Its excess noise factor is low enough, *i.e.* F-values are spread between 2.2 and 2.5 for the APD-gain range of 150–350 (see Fig. 9).

These characteristics of the Advanced Photonics Inc. APD together with the improved light yield in the new Shashlyk module allow us to reduce the photostatistics contribution to the energy resolution of the calorimeter to the negligible level of $0.7\%/\sqrt{E\ (\mathrm{GeV})}$, while the electronic noise contribution of ≤ 0.4 MeV is also negligible.

3 Experimental Study of the Calorimeter Prototypes

3.1 Test beam

Test measurements of the prototype of a Shashlyk calorimeter with energy resolution of $3\%/\sqrt{E\ (\mathrm{GeV})}$ have been made with the photon beam from the Laser Electron Gamma Source (LEGS) facility [18], which is located on the X5 beam line of the X-ray ring at the National Synchrotron Light Source (NSLS) at Brookhaven National Laboratory (BNL). A schematic drawing of the tagged photon beam and detector setup for these measurements is shown in Fig. 16. The photon beam was produced by Compton backscattering of an Ar-ion laser incident on the 2.58-GeV electrons in the storage ring of the NSLS, resulting in a continuous photon beam with an energy range of 150

to 400 MeV. The energy of each beam photon was known by detecting the Compton scattered electron.

The tagged photon beam had a mean intensity of $\sim 3 \times 10^5$ Hz, a size of $\sim$1.5 cm at the detector position, and an angular spread of $\sim$2 mrad. The photon energy was tagged with an accuracy of $\delta E_\gamma / E_\gamma \approx 1.5\%$. The timing accuracy of the tagging spectrometer was $\simeq$1 ns. Several monochromatic photon energy lines in the range of 220–370 MeV were triggered in our measurements.

3.2 Calorimeter Prototypes

Two arrays of 3×3 prototype modules with the same sampling were tested.

The first array (prototype 1) contained 9 conventional (paper between lead and scintillator) modules with the 30-mm-diameter, green-sensitive PMT-9903B of *Electron Tube Inc.*

The second array (prototype 2) contained a nonet of new design modules equipped with the 16-mm-diameter APD 630-70-74510 of *Advanced Photonix Inc.* An instrumented APD-unit is shown in Fig. 14, which includes the APD itself, the APD amplifier, and the APD HV bias.

For these test measurements, a fast low-noise CSA has been designed to optimize the signal-to-noise ratio and the double-pulse resolution. The overall linear chain of the amplifier is shown in Fig. 15. It consists a charge-sensitive preamplifier and a shaper-amplifier. The charge-sensitive part of this scheme is designed as a cascode amplifier with two parallel-connected low-capacitance JFET transistors to improve the signal/noise ratio. The second stage of the amplifier provides a cancellation of the signal tail by a "pole-zero cancellation" network ($\tau \simeq 18$ ns), and also provides an additional amplification of the signal. Two types of the low-capacitance input JFET transistors have been considered for this amplifier: the Russian 2P341A transistor and the Japanese SK2394/YJ5 transistor. Both transistors are characterized by a high transconductance ($g_m > 20$ mA/V) for moderate drain current and low input capacitance ($C_{\rm JFET} < 10$ pF). The ENC of the designed amplifier for both versions of the input JFETs was measured for several detector capacitances up to 150 pF. Results are shown in Fig. 11. We used the amplifier with two SK2394/YJ5 transistors in the test beam measurements.

Because the new Calorimeter photodetector (APD) draws only its photocurrent with typical values much less than 0.1 mA, an economic way to build the Calorimeter HV system is to develop an active, compact, low-current individual HV-unit, mounted directly into each APD housing. This kind of HV system eliminates expensive and bulky HV cables and connectors, lowers the

power consumption per individual power supply, and reduces the electrical HV hazard associated with traditional HV supplies.

In the test measurements, two types of APD HV supplies were tested: traditional HV supply - a *BERTAN* 377P of NIM standard and a HV "built-in" unit (see Fig. 14) with a new commercial, compact, regulated and programmable LV-HV converter (C20), produced by EMCO. The stability of both bias systems was better than 0.1 V/hour, which provided an APD gain stability better than 0.3%.

3.3 Cooling

The photodetectors (APD) of the Prototype 2 were placed in a thermo-isolated cooling unit. During the test period of 24 hours, the APD temperature was keeped at 18° C, variation did not exceed 0.2° C. Such cooling system allowed us to neglect the temperature dependent effects in data analysis.

3.4 Readout

One of the goal of the photon beam measurements was testing of the readout prototype for KOPIO experiment. The readout electronics had to be capable of measuring energies with a digitization uncertainty of 0.5 MeV in a dynamic range of 2–1000 MeV, and the time of arrival with respect to the beam microbunch clock with an uncertainty of less than 100 ps. Operation of this readout electronics had to be completely pipelined with no dead time. It had to be also capable of forming and discriminating the total energy signals and the total number of hits in the Calorimeter. Taking into account these performance requirements for energy and timing resolutions of the calorimeter with PMT or APD readout and the experiment's requirement to study effective and economic way for the energy and timing measurement, we have chosen for these test measurements two parallel readout schematics: an investigated readout, based on 8-bit 140-MHz WFDs, which have been developed by Yale University, and a reference readout, based on conventional 12-bit LeCroy QDCs to check performance of new-developed WFDs.

3.5 Calibration and Monitoring

To achieve the required energy resolution of the KOPIO Calorimeter, $\sim 3.0\%/\sqrt{E}$, an appropriate pre-calibration and monitoring system must be developed.

We have used vertical cosmic-ray muons for pre-calibration of the calorimeter prototypes, as we did in Experiment E865 [4]. The accuracy of this pre-calibration was estimated to be about 4%.

To monitor the calorimeter prototypes performance during our measurements and to correct the variation of the photodetector gains with accuracy of 0.4%, we have used a prototype of the KOPIO calorimeter monitoring system that employs the high-brightness Light Emitting Diodes (LEDs NSPB-310A) to inject their blue light into the scintillator via a clear fiber. This monitoring system was based on an electronic method of stabilization of the LED light output by means of an optical feedback provided by a PIN photodiode as shown in references [23] and [24].

Preliminary and beam-test studies of a described monitoring system have shown, that this system has satisfied a number of our specific requirements:

- short light pulse duration —less than 15 ns;
- variable light pulse intensity ($5,000 \div 20,000$ photons/channel);
- variable pulse repetition rate (up to $1MHz$);
- high long-term and short-term temperature stability — better than 0.1%;
- small variation in the flash amplitude —less than 0.2%.

The monitoring system can also serve as a pre-calibration of the module readout chain at the 10% level.

For final calibration of the prototypes we have used the photon beam. Both calorimeter prototypes were mounted on platforms that could be moved horizontally and vertically with respect to the beam line, so that each prototype module could be calibrated (with an accuracy $\leq 1\%$) by using the 250-MeV photon beam that passed through the central region of the module at normal incidence.

4 Experimental Results

4.1 Calorimeter prototype response

The pedestal response, the sum of electronic noise and pile-up for individual modules, was measured during the test runs by using a special gate signal that was shifted from the photon timing by up to 1 μs. The contribution of this effective noise to the energy resolution was (0.5 ± 0.1) MeV for the case of the "APD+QDC" readout. The total equivalent noise for the "APD+WFD" readout was (1.0 ± 0.2) MeV. This value is twice as large as that for the first

one due to a digitization uncertainty of the 8-bit WFD. The lowest equivalent noise, (0.2 ± 0.1) MeV, was obtained with the PMT-9903B tubes.

The typical response of the nonet of the "APD+WFD"-instrumented modules to a 340-MeV photon hitting the nonet at the center of the central module, is shown in Fig. 17. The measured signal distribution in the WFD was fit by a function $Af(t - t_0) + P$, where $f(\tau)$ is an experimentally determined pulse shape function. The signal amplitude A, signal time t_0, and pedestal P were free parameters in the fit.

4.2 Energy Resolution

The energy resolution was measured for both prototypes 1 and 2. The photon beam was directed to the center of the module nonets. Energy spectra of 250- and 370-MeV photons in the Shashlyk nonet with the APD+WFD readout are shown in Fig. 18. Note the good agreement between Monte-Carlo and experimental distributions, that gives us a confidence that our simulation model, which includes effects of the beam energy spread, energy loss upstream calorimeter, photon shower evolution, light collection in scintillator tiles and light transmission in WLS fibers, the response of the photodetector, and noise of the entire electronic chain, properly reproduces the actual calorimeter response.

The energy-resolution results for various prototypes of calorimeters are displayed in Fig. 19. The best result was achieved for the "APD+WFD" readout. A fit to these experimental data gives

$$\sigma_E/E = (1.96 \pm 0.1)\% \oplus (2.74 \pm 0.05)\%/\sqrt{E\ (\mathrm{GeV})}\,,$$

where $\oplus$ means a quadratic summation. The relatively large constant term of 2% may be explained by the short, 15.9-X_0 radiation length of the module. The constant term may be easily improved by increasing length of the module. However, this term is not essential for the photon energy range of $100 \div 1000$ MeV.

We may note, that the model developed for the simulation of a Shashlyk module accurately predicts the energy resolution from the module parameters.

4.3 Time Resolution

To estimate the time resolution, we measured the time difference for the signals produced by the same shower in two neighbor modules. By using this mea-

surement technique, the 340-MeV photon beam was directed between central module (#5) and left module (#4). The photon energy distributions in the nonet of the Shashlyk modules during the timing measurements, are shown in Fig. 21.

Only events with the full photon energy ($E_4 + E_5 = 320 \pm 20$ MeV) deposited in these two modules were selected for analysis. The dependence of the time difference dispersion on the energy deposited in one module is shown in Fig. 22. The time difference resolution drops significantly if one of the two deposited energies is close to zero or, alternatively, if one of the energies is close to 340 MeV. Assuming that both modules have the same time resolution $\sim 1/\sqrt{E}$, we have obtained from Fig. 22

$$\sigma_T = (90 \pm 10)\ \text{psec}/\sqrt{E\ (\text{GeV})}\,.$$

The signals we use to evaluate the time resolution are strongly correlated because they are produced by the same electromagnetic shower. This may result in a wrong value of the time resolution. For example, the contribution of the longitudinal fluctuation of the shower is suppressed in such measurements. To ensure that our test-beam result does not underestimate the actual time resolution, we carried out a Monte Carlo simulation of the time resolution.

To simulate the time response and time resolution of a Shashlyk module, a Monte Carlo model was newly developed for the evolution of the light signal in a module. Ionization produced by a charged particle in a scintillator tile survives several transformations before the corresponding light signal appears at the entrance of a photodetector. Ionization produced by an electromagnetic shower occur at different space points and different times, resulting in a time spread of the photoelectron emission in the photodetector. In addition, the actual emission delays depend randomly on the decay times in the scintillator and the WLS fibers, light collection time in the scintillator fiber, and the propagation of light in the WLS fiber. The following effects have been taken into account in the model:

- the space-time distribution of hits in the Shashlyk module scintillator;
- the decay time in scintillator;
- the light collection time in the scintillator tile;
- the decay time in WLS fibers;
- the effective velocity of light propagation in WLS fibers;
- the light attenuation length in WLS fibers;
- bending loss in the WLS fiber loop; and
- the response function of the detector chain, including photodetector (APD), preamplifier, cables and WFD.

The simulated response of the Shashlyk module for the 250-MeV photons is

shown in Fig. 23. The shape of the simulated signal in a Wave Form Digitizer matches well an experimentally measured signal shown in Fig. 17.

In the Monte-Carlo simulation of these measurements, we have obtained

$$\sigma_{T4-T5}(E_4 = E_5) = 280 \text{ ps}$$

which is in a good agreement with the experimental value of 285 ps (see Fig. 22).

The Monte-Carlo simulations of the mean measured time and measured time dispersions depending on type of particle and its energy is shown in Fig. 24. To understand the behavior of mean time values we should note that by fitting the signal shape in WFD we actually measure the center of gravity of the signal time distribution. The total time delay in the fiber does not depend on the position of the hit in scintillator if we neglect the light attenuation in the fiber. This means, that in such approximation, the relative delay of the measured hit is solely defined by the time at which hit ocured.

As one can see from Fig. 24 our method of determination of the time resolution, based on the measurement of time difference in the neibohour modules is adequate to the true time resolution.

4.4 Photon Detection Inefficiency

To estimate the photon detection inefficiency due to fiber holes, a prototype 1 nonet was located behind the prototype 2 array. The absence of a signal in the front array, while the total photon energy was deposited in the second, was interpreted as a penetration of the photon through the first prototype without interaction, *e.g.* through a fiber hole. Photons of 250 MeV were directed onto the face of the first array. The measured dependence of the photon detection inefficiency on the beam incident angle is compared with the simulation in Fig. 25. The relatively coarse step in the measured angles does not allow us to accurately compare the experimental results with the simulation. However, our measurements clearly indicate that the effect of the WLS fiber holes is negligible if the incident angle is ≥ 5 mrad. For such angles, our experimental results agree well with the probability of photon interactions in about 8.25 cm of lead and 45 cm of scintillator.

4.5 Long-term APD Stability

The APD and PMT gains were monitored by using LED signals during the run time of 24 hours to test the long-term stability of the photodetector gain. Experimental data, illustrating the long-term stability of the APD and PMT readout of the calorimeter prototypes, are shown in Fig. 26. One can see in the upper picture of this figure a rate effect for the PMT-9903B after changing the photon beam rate (intensity) from 0 kHz to 300 kHz. No APD gain dependence on the photon beam intensity was observed after changing the photon beam rate from 0 kHz to 300 kHz. The variation of the APD gain did not exceed 1%.

5 Summary

We Modules for a KOPIO Shashlyk Calorimeter with energy resolution

$$\sigma_E/E = (1.96 \pm 0.1)\% \oplus (2.74 \pm 0.05)\%/\sqrt{E\ (\mathrm{GeV})}\,,$$

time resolution

$$\sigma_T = (90 \pm 10)\ \mathrm{psec}/\sqrt{E\ (\mathrm{GeV})}\,,$$

and a photon detection inefficiency due to fiber holes of

$$\epsilon \leq 5 \times 10^{-5}\ \ (\Theta_{\mathrm{beam}} > 5\ \mathrm{mrad})$$

have been constructed and experimentally tested. The characteristics experimentally determined for the Calorimeter prototype well meet the design goals of the experiment.

To optimize the Calorimeter readout design, a Monte Carlo simulation model of the light transmission in scintillator tiles and WLS fibers, the response of the photodetector, and noise of the entire electronic chain. This model accurately describes the experimental data.

The Shashlyk calorimeter described in this paper was designed for the KOPIO experiment The conceptual design of the KOPIO calorimeter has been done [25], including the design of the Calorimeter construction, readout scheme, monitoring and calibration system. Main components of the KOPIO calorimeter have been tested and Calorimeter was ready for the manufacturing. How-

ever, due to the stopping of the KOPIO experiment, the production of the Calorimeter was not started.

Through calculation and experimentation, we have improved the energy resolution of Shashlyk modules over the past several years. We note this progress in Table 4 and Fig. 20.

Acknowledgments

We must not forget to thanks ...

References

[1] G.S. Atoyan, *et al.*, Nucl. Instr. and Meth, A **320**, 144 (1992).

[2] I.-H. Chiang et al., *AGS Experimental Proposal 926* (1996).

[3] G.S. Atoian, *et. al.*, Nucl. Instr. and Meth. A **531**, 467 (2004).

[4] R. Appel *et. al.*, Nucl. Instr. and Meth. A **479**, 349 (2002).

[5] L. Aphecetche, *et al.* [The PHENIX Collaboration] Nucl. Instr. and Meth. A **499**, 521 (2003).

[6] G. Avoni *et al.* [The HERA-B ECAL Collaboration], Nucl. Instr. and Meth. A **461**, 332 (2001).

[7] F. Muheim [For the LHCb Collaboration], Nucl. Instr. and Meth. A **462**, 233 (2001).

[8] GEANT, Detector description and simulation tool, CERN Program Library, Long Writeup W5013 (1994).

[9] G. Atoian *et al.*, *Test beam study of the KOPIO Shashlyk calorimeter prototype*, in Proceedings of the Eleventh International Conference on Calorimetry in Particle Physics, Perugia, Italy, 29 March – 2 April, 2004, Editors Claudia Cecchi, Patrizia Cenci, Pascuale Lubrano, and Monica Pepe, World Scientific, 2005, p.55.

[10] http://www1.ihep.su/ihep/ihepsc/index.html .

[11] Kuraray Co., LTD, *Scintillation materials. Plastic fibers.*

[12] S.P. Stoll, PHENIX Note #245 (1996).

[13] I.G. Britvich *et al.* Instr. Exp. Tech. **44**, 472 (2001).

[14] I.G. Britvich *et al.* Instr. Exp. Tech. **45**, 644 (2002).

[15] J. Marler *et al.*, Nucl. Instr. and Meth. **449**, 311 (2000).

[16] R.J. McIntyre, IEEE Trans. Electron Devices **ED-13**, 165 (1966).
P.P. Webb, R.J. McIntyre, J. Conradi, RCA Review **27**, 164 (1966).
R.J. McIntyre, IEEE Trans. Electron Devices **ED-19**, 703 (1972).

[17] R.J. McIntyre, *A New Look at Impact Ionization-Part I: A Theory of Gain, Noise, Breakdown Probability, and Frequency Response*, IEEE TRANSACTIONS ON ELECTRON DEVICES, VOL. 46, NO. 8, 1623 (1999).
P. Yuan *et. al.*, *A New Look at Impact Ionization-Part II: Gain and Noise in Short Avalanche Photodiodes*, IEEE TRANSACTIONS ON ELECTRON DEVICES, VOL. 46, NO. 8, 1632 (1999).

[18] D. H. Dowell et al., Prog. Rep. BNL 37623 (1985), p. 29.

[19] http://www.emcohighvoltage.com/

[20] A.L.Wintenberg et al., PHENIX Project, internal paper, 2000.

[21] The LHCb Technical Proposal. CERN/LHCC 98-4.

[22] *"The Front-End Electronics for LHCb calorimeters"*, LHCb 2000-028.

[23] W.L. Reiter *et. al.*, Nucl. Instr. and Meth. **173**, 275 (1980).

[24] A. Fyodorov *et. al.*, Nucl. Instr. and Meth. **A413**,352-356 (1998).

[25] KOPIO CDR report.

Table 1
Parameters of the $3\%/\sqrt{E\ (\mathrm{GeV})}$ KOPIO prototype module.

Lateral segmentation	110×110 mm^2
Scintillator thickness	1.5 mm
Spacing between scintillator tiles	0.350 mm
Lead absorber thickness	0.275 mm
Number of layers	300
WLS fibers per module	72×1.5 m =108 m
Fiber spacing	9.3 mm
Hole diameter (lead/scint.)	1.3 mm
Diameter of WLS fiber (Y11-200MS)	1.0 mm
Fiber bundle diameter	14.0 mm
External wrapping (TYVEK paper)	150 μm
Effective radiation length, X_0	34.9 mm
Effective Moliere radius, R_M	59.8 mm
Effective density	2.75 g/cm^3
Active depth	555 mm (15.9 X_0)
Total depth (without photodetector)	650 mm
Total weight	21 kg

Table 2
Scintillators tested for the KOPIO Shashlyk module. The "light yield" is the amount of light produced in the scintillator without respect to the light collection efficiency, while "MIP light yield" is the detected light signal per minimum ionization particle passing through the scintillator tile. The "effective attenuation length" was measured for a thin, 1.5-mm scintillator tile.

Scintillator: Polystyrene+Fluor1+Fluor2 Manufacturer	Light yield (% of Anthracene)	Effective attenuation length in tile (cm)	MIP light yield (p.e. per tile)
PSM115+1.5%pTP+0.04%POPOP TECHNOPLAST, 1998	53 ± 6	4.3 ± 0.2	4.4 ± 0.3 100%
BASF158K+1.5%pTP+0.04%POPOP IHEP, 2001	56 ± 6	5.0 ± 0.2	5.6 ± 0.3 $(127 \pm 10)\%$
BASF165H+1.5%pTP+0.04%POPOP IHEP, 2001	56 ± 6	5.3 ± 0.3	6.4 ± 0.3 $(145 \pm 10)\%$
BASF143E+1.5%pTP+0.04%POPOP IHEP, 2002	54 ± 6	5.4 ± 0.2	7.1 ± 0.3 $(161 \pm 10)\%$

Table 3
Some experimental and catalog parameters of the green-sensitive PMT-9903B and three pre-selected large-area APDs. Data for a well-known small-area APD, produced by Hamamatsu Corporation, are shown for comparison.

Item	*PMT*	*APD*			
	9903B *(Electron Tubes, Inc.)*	630-70-74-510 *(Advanced Photonix, Inc.)*	S1315 *(RMD Instruments, Inc.)*	C30703E *(Perkin-Elmer, Inc.)*	S8664-55 *(Hamamatsu Photonics, K.K.)*
Active area (S)	~ 600 ($\oslash 30$) (mm^2)	~ 200 ($\oslash 16$) (mm^2)	169 (13×13) (mm^2)	100 (10×10) (mm^2)	25 (5×5) (mm^2)
Quantum eff. (Q) at $\lambda = 550$ nm	19 (%)	94 (%)	66 (%)	76 (%)	81 (%)
Gain (M)	$\geq 10^5$	≤ 1000	≤ 10000	≤ 200	≤ 200
Specific capacitance (C)	~ 0.01 (pF/mm^2)	~ 0.65 (pF/mm^2)	~ 0.71 (pF/mm^2)	~ 1.0 (pF/mm^2)	~ 3.2 (pF/mm^2)
Series resistance (R_S)	– –	~ 10 (Ohm)	~ 40 (Ohm)	~ 15 (Ohm)	~ 5 (Ohm)
Density of surface current (I_S/S)	≤ 5 (pA/mm^2)	≤ 300 (pA/mm^2)	≤ 1700 (pA/mm^2)	≤ 800 (pA/mm^2)	≤ 100 (pA/mm^2)
Density of bulk current (I_B/S)	≤ 0.1 (pA/mm^2)	≤ 3 (pA/mm^2)	≤ 4 (pA/mm^2)	≤ 5 (pA/mm^2)	≤ 6 (pA/mm^2)
Excess noise factor (F)	~ 1.5 (M$\simeq 10^5$)	~ 2.2 (M$\simeq 100$)	~ 2.1 (M$\simeq 100$)	~ 3.6 (M$\simeq 100$)	~ 2.7 (M$\simeq 100$)
k-factor	–	~ 0.002	~ 0.001	~ 0.015	~ 0.007
Width (FWHM) of multiplication zone	–	~ 65 (μm)	~ 75 (μm)	~ 10 (μm)	~ 12 (μm)
Intensity of E-field inside of M-zone	–	~ 230 (kV/cm)	~ 210 (kV/cm)	~ 340 (kV/cm)	~ 380 (kV/cm)

Table 4
Evolution of the energy resolution of Shashlyk modules.

Year of production	Number of layers	Lead thickness (mm)	Scintillator thickness (mm)	Energy resolution $\left(\times\sqrt{E\ (\mathrm{GeV})}\right)$
1991 (E865)	60	1.4	4.0	8.0%
1996 (E923)	120	0.7	3.0	5.8%
1998 (E926)	240	0.35	1.5	4.0%
2003 (KOPIO)	300	0.275	1.5	3.0%

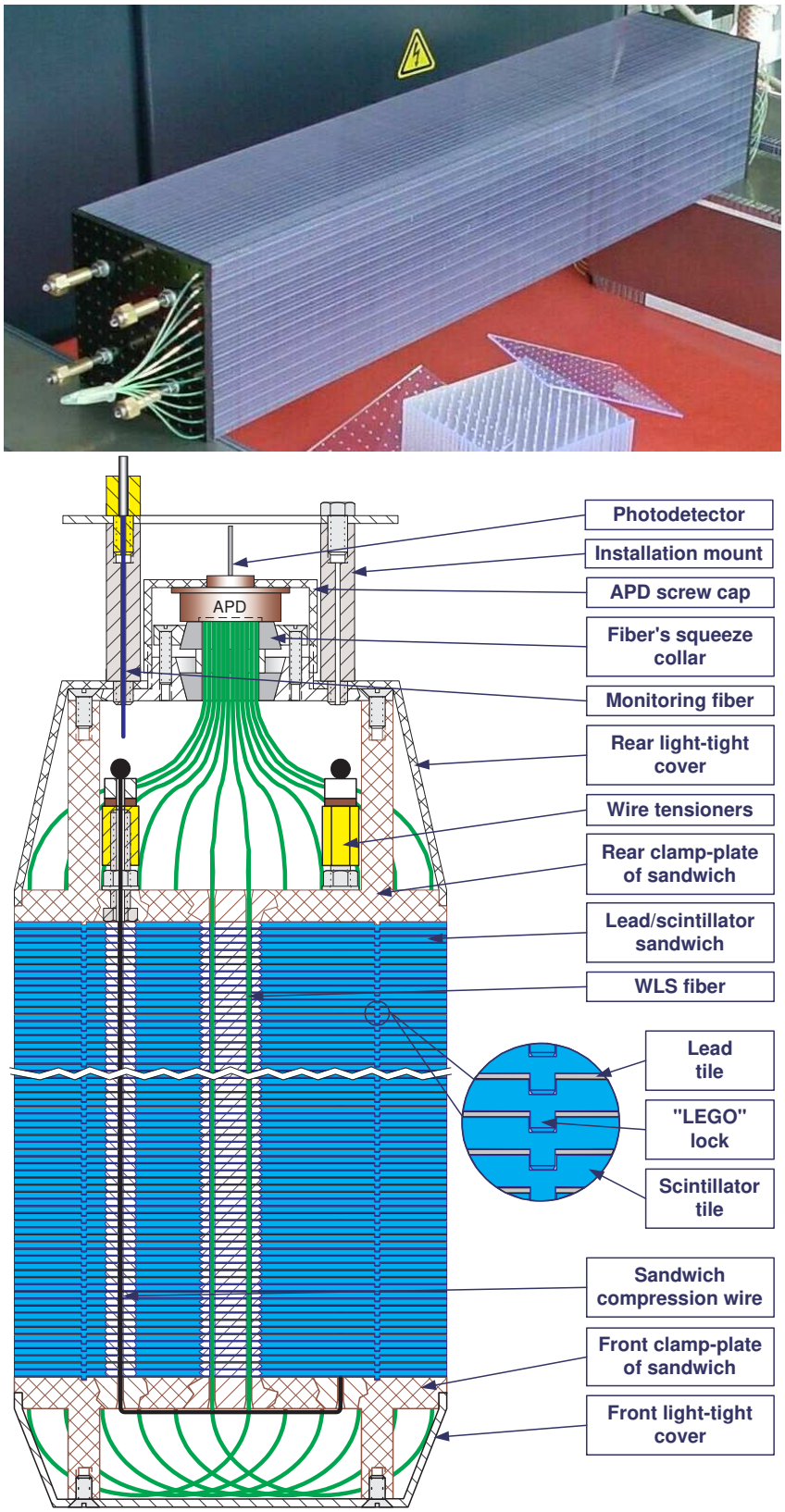

Fig. 1. A Shashlyk module assembly is shown in the top picture. The module design in shown in the bottom picture.

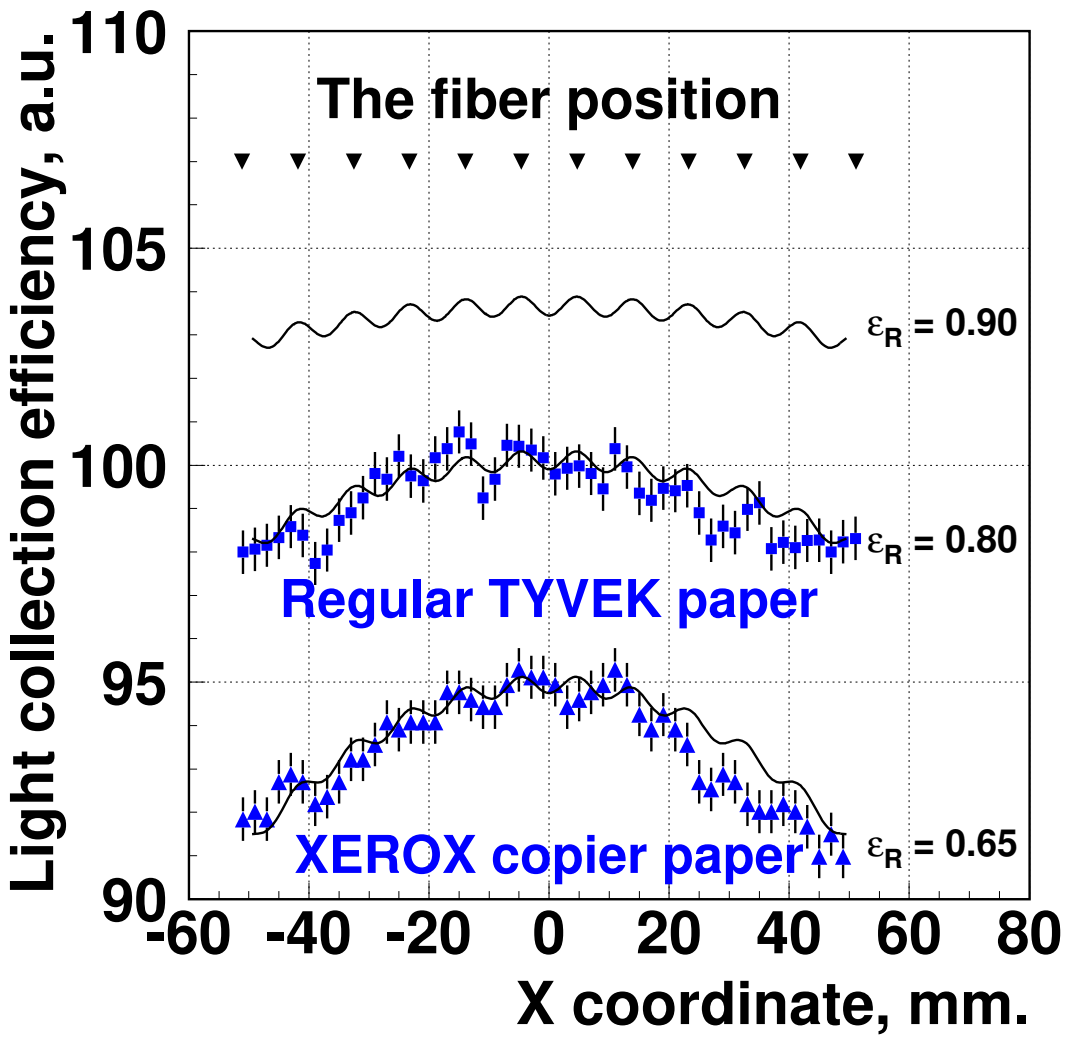

Fig. 2. The dependence of the light collection efficiency on the X-coordinate of the point-like light source. Solid lines are the simulations for the specified reflection efficiencies ε_R of the wrapping material.

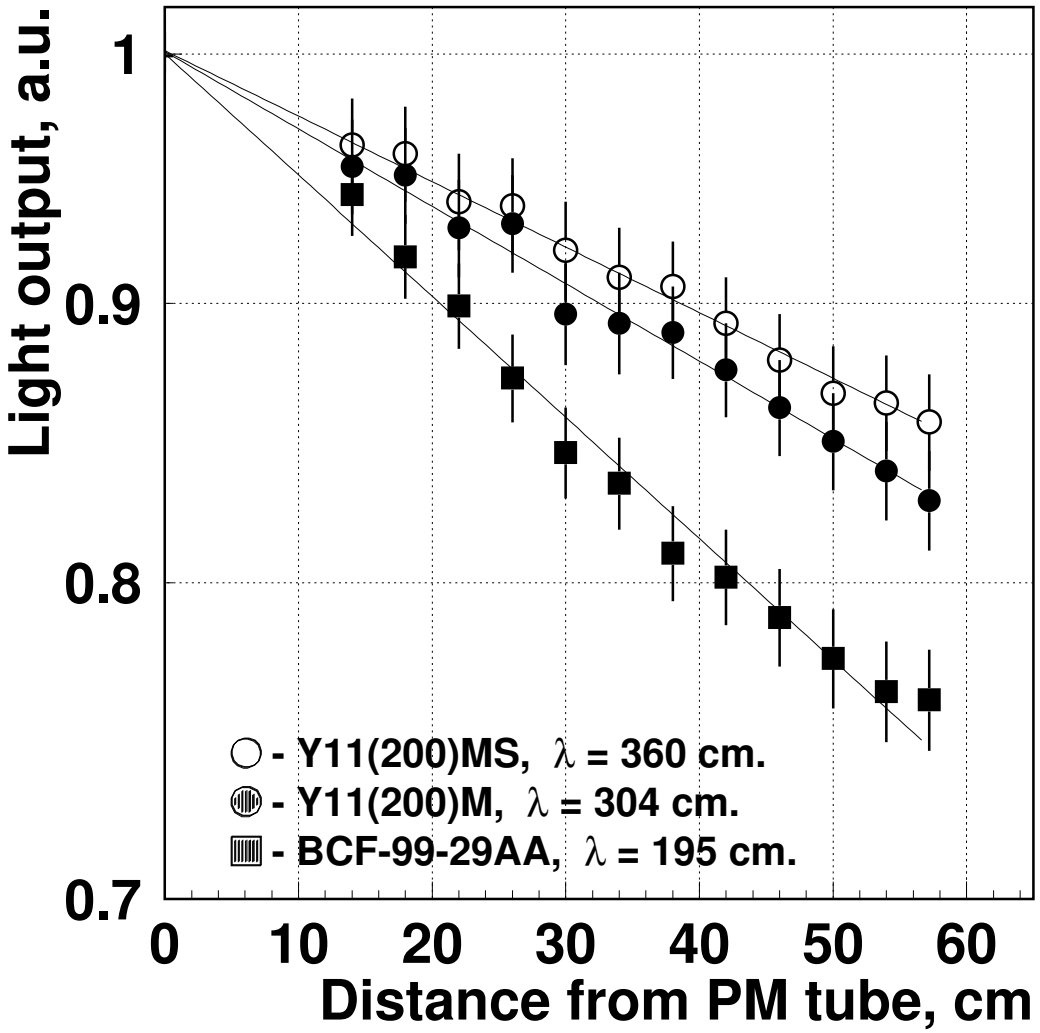

Fig. 3. The effective attenuation of the light in the fibers of Shashlyk module. Experimental data (marks) are fit by the exponential dependence $\exp(-x/\lambda)$ (solid lines), where x is the distance to the PMT and λ is the effective attenuation length. Measurements were made by using a collimated light source and muons that penetrated the modules transversely.

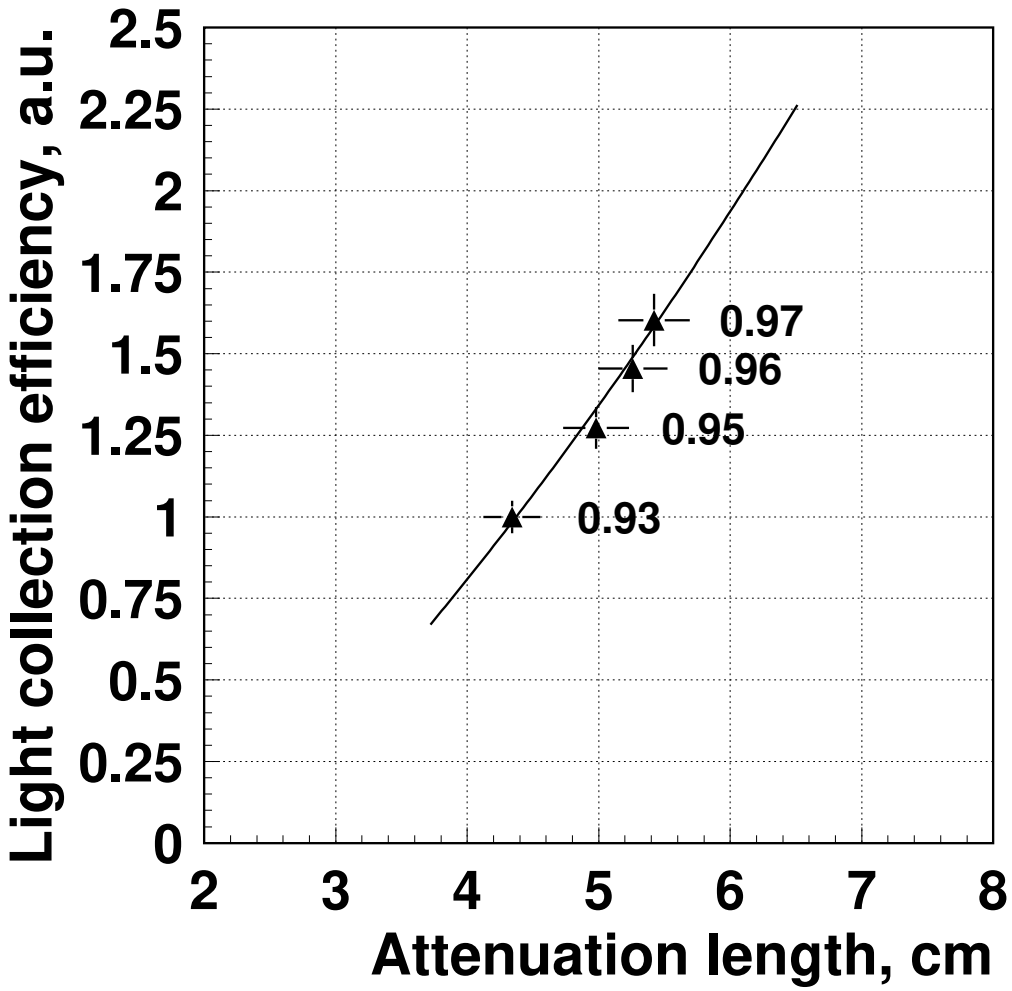

Fig. 4. The parametric dependence of the light collection efficiency on the effective attenuation length due to the reflection efficiency. The solid line is the result of a calculation based on the model of Ref. [3]. The experimental results are taken from Table 2. For each scintillator, the calculated reflection efficiency is displayed.

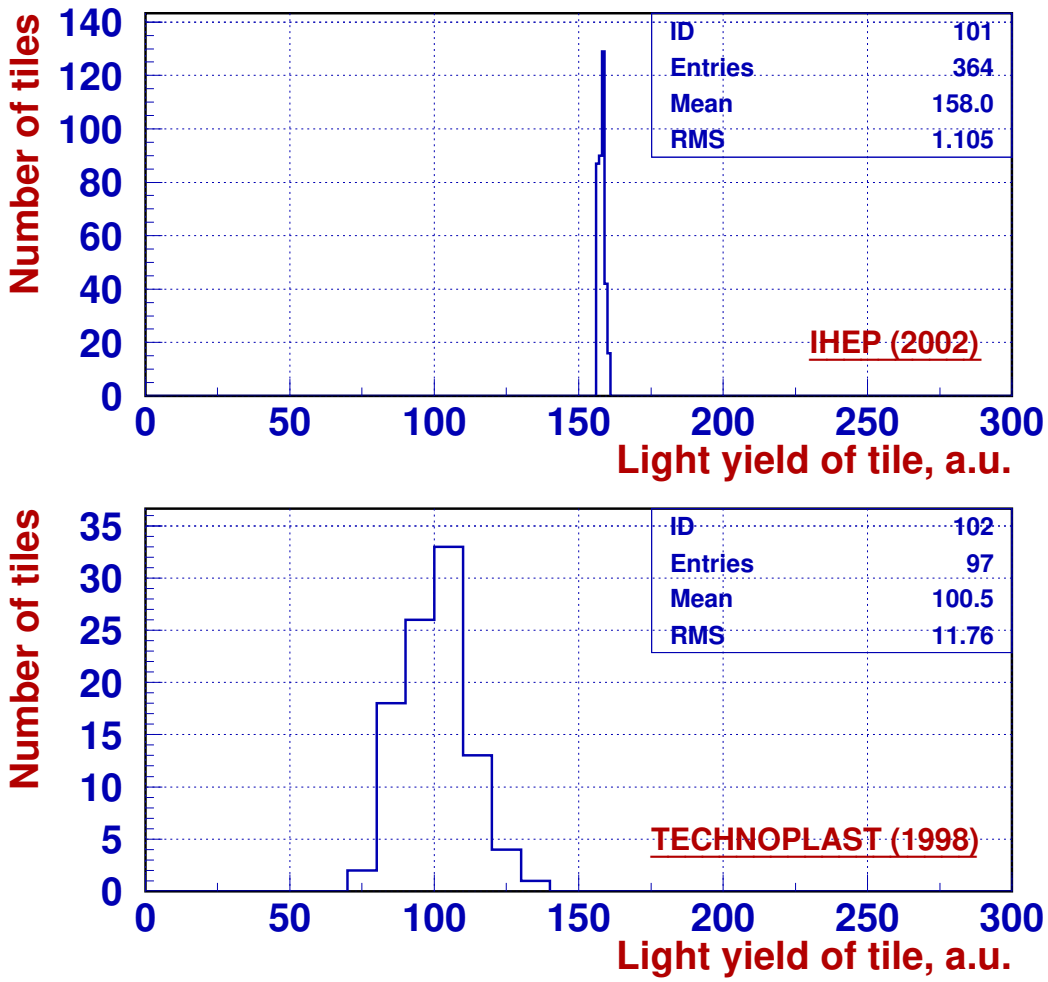

Fig. 5. Comparison of the light-yield spread for scintillator tiles used in the 1998 (bottom) and 2003 (top) Shashlyk modules prototypes.

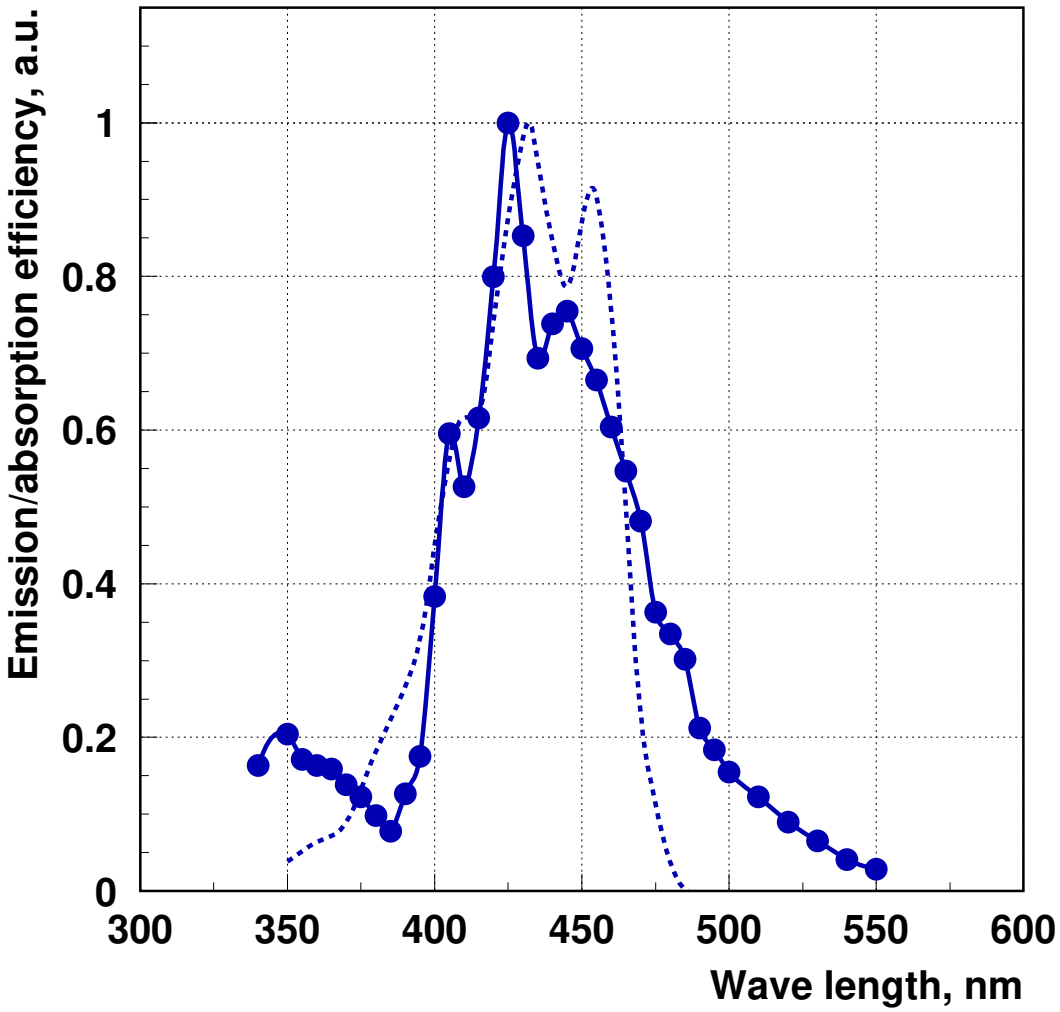

Fig. 6. The closed circles and solid line are the measured emission spectra of the BASF143E-based scintillator. The dashed line is the absorption spectrum of KURARAY Y11(200)MS WLS fibers.

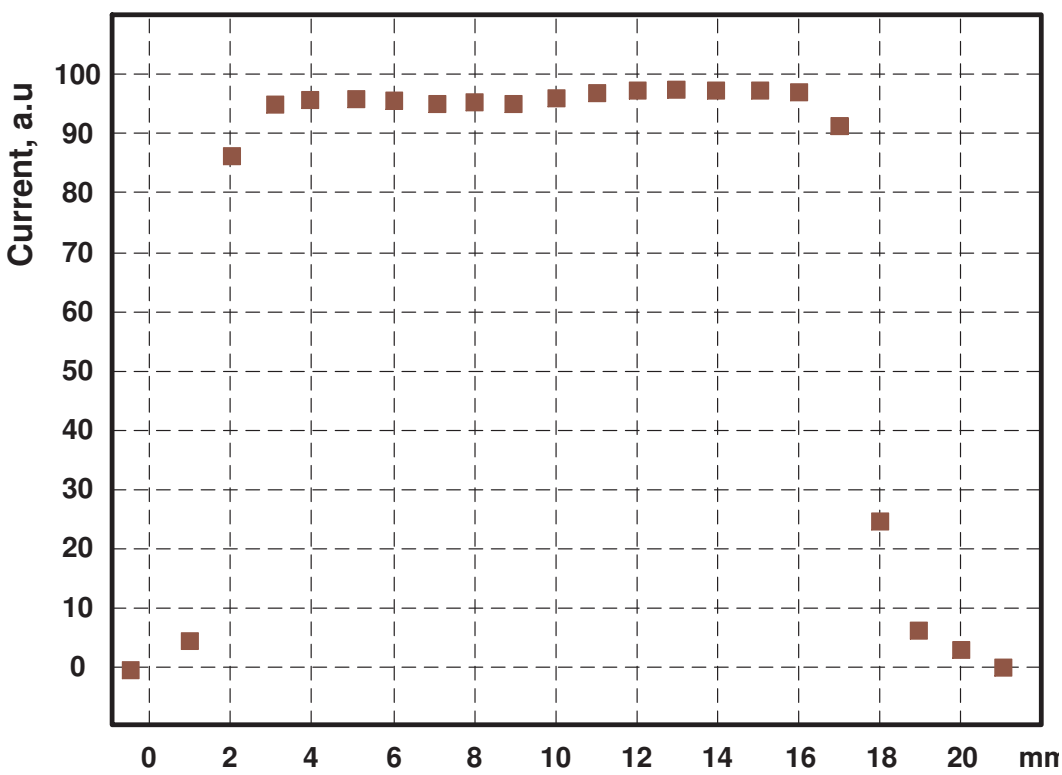

Fig. 7. Variation in current measured across a 16-mm-diameter APD-630-70-74-510.

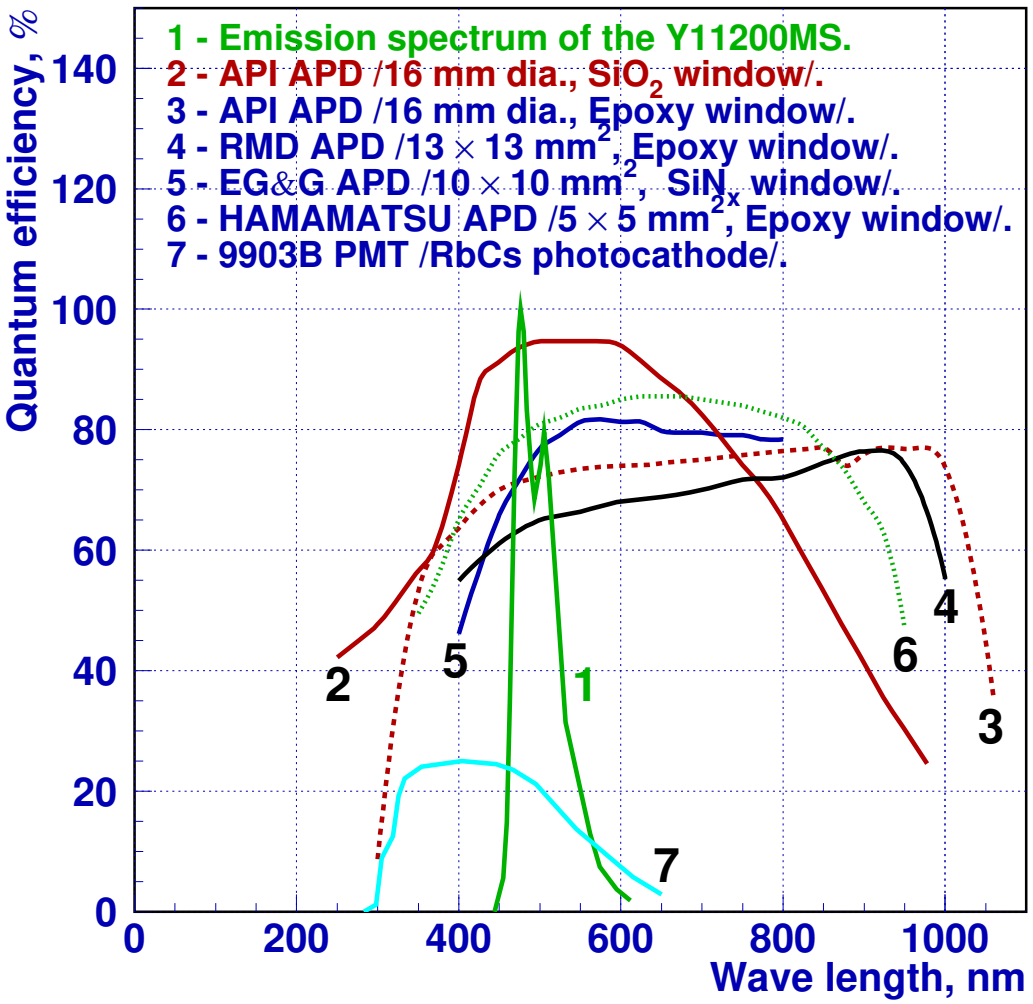

Fig. 8. The quantum efficiency of various APDs and the 9903B PMT *vs.* the light wavelength. An emission spectrum of the Kuraray Y11200MS WLS fiber (a solid green line) is shown in the same picture.

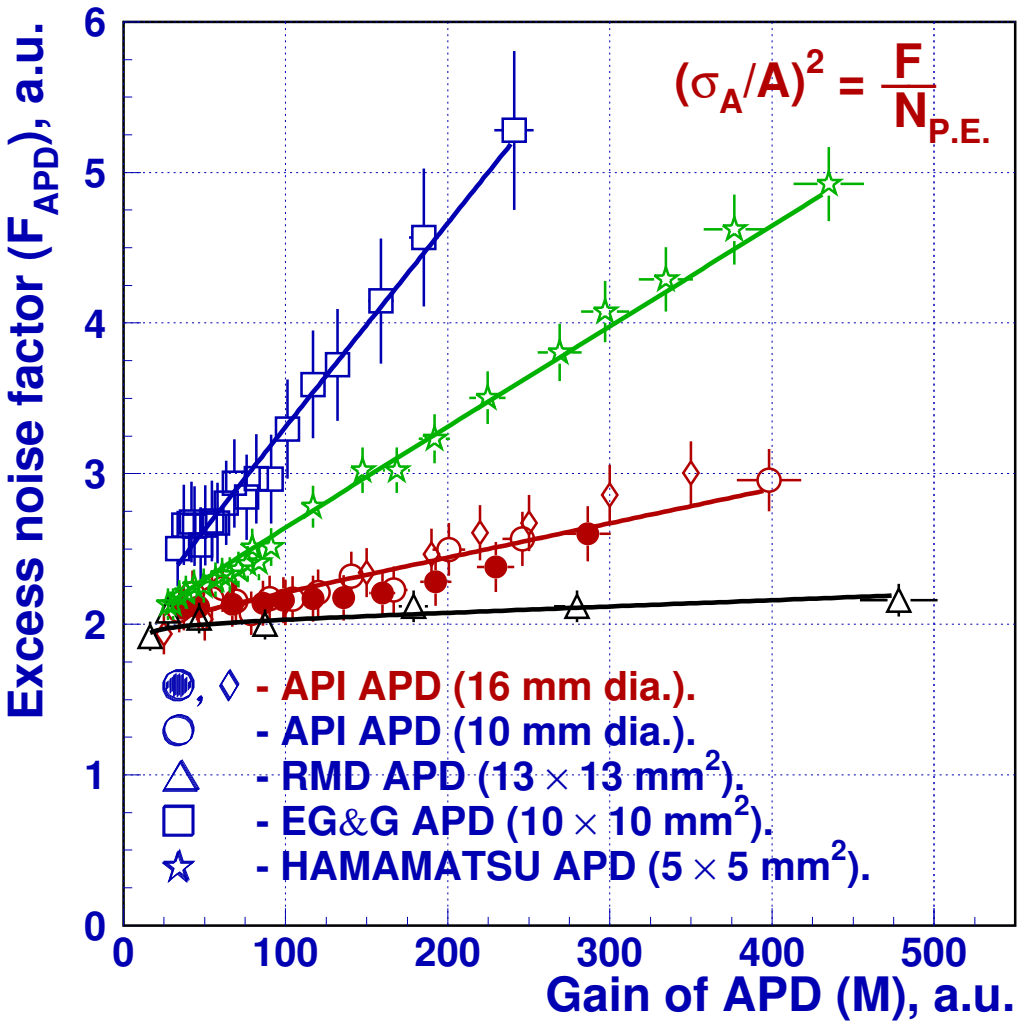

Fig. 9. The APD excess noise factor *vs.* the APD gain for various pre-selected APDs.

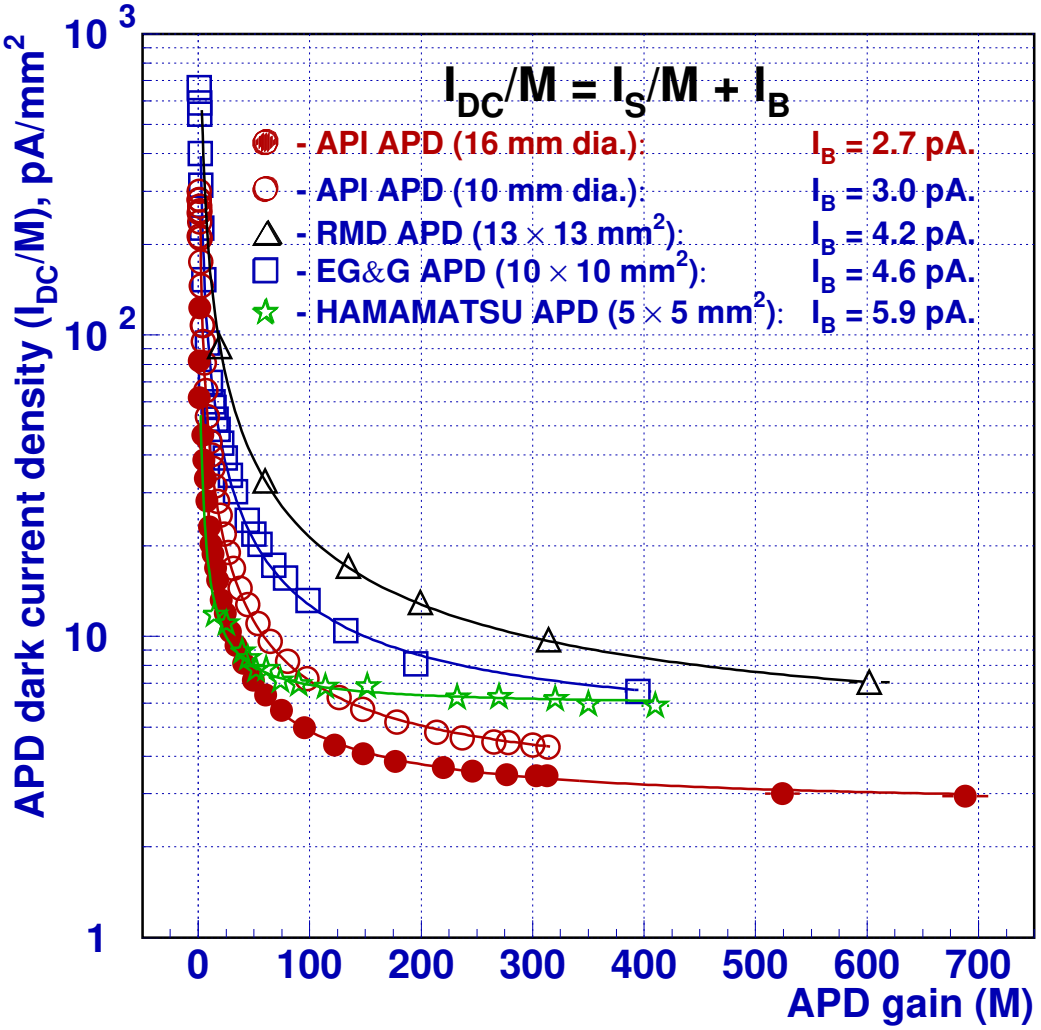

Fig. 10. The APD dark current densities as a functions of gain for the various pre-selected APDs. KOPIO data.

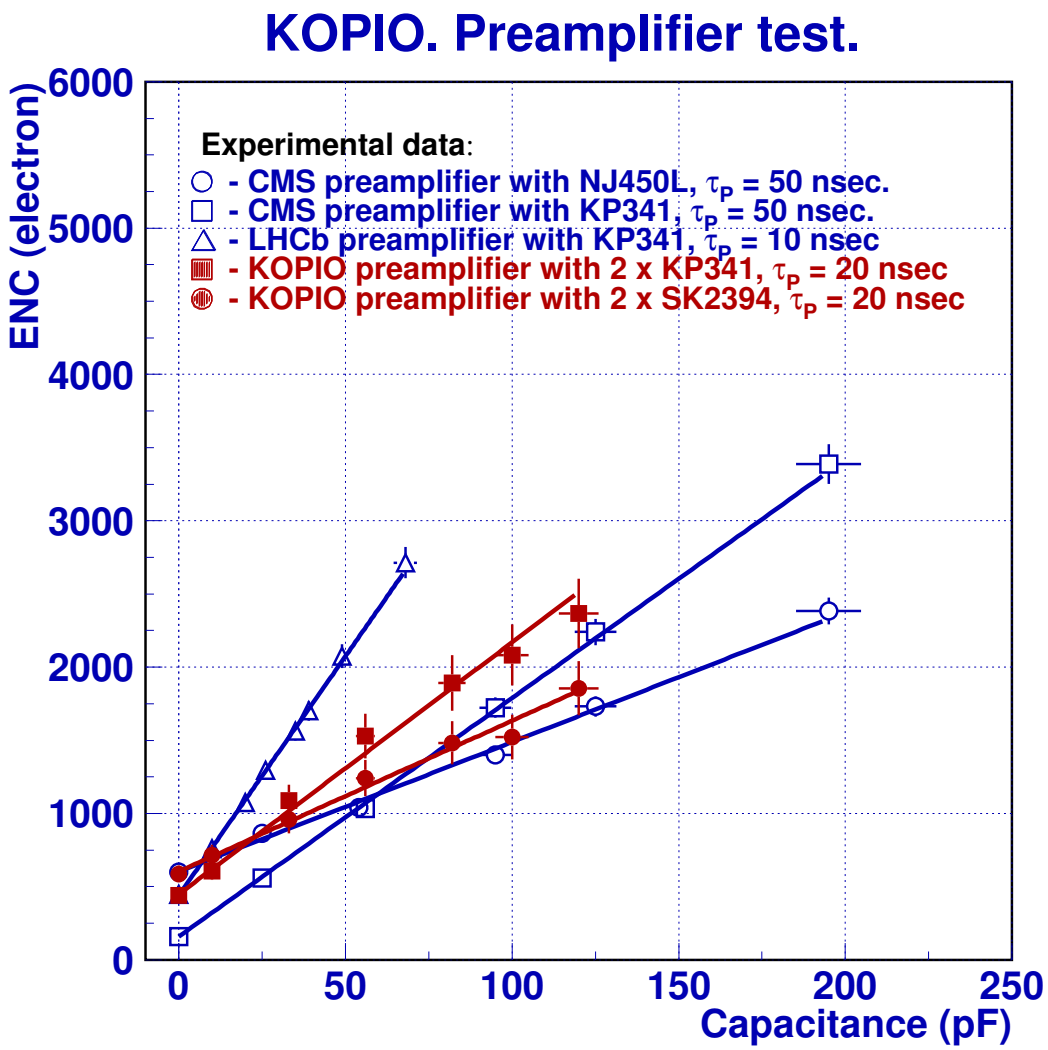

Fig. 11. Equivalent Noise Charge (ENC) *vs.* the input capacitance for some fast Charge Sensitive Amplifiers. Integration time was 100 ns in all measurements.

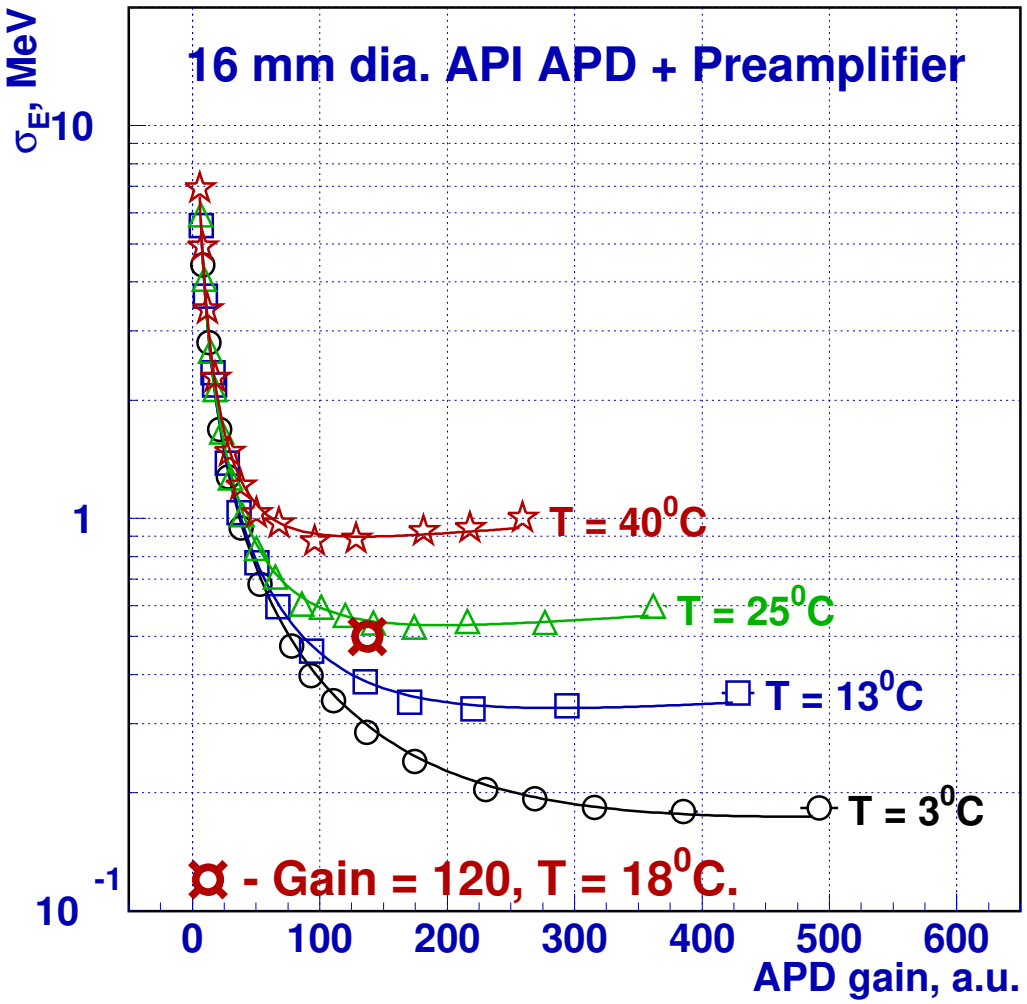

Fig. 12. Equivalent energy noise of an APD/amplifier chain *vs.* the APD gain for various environment temperatures.

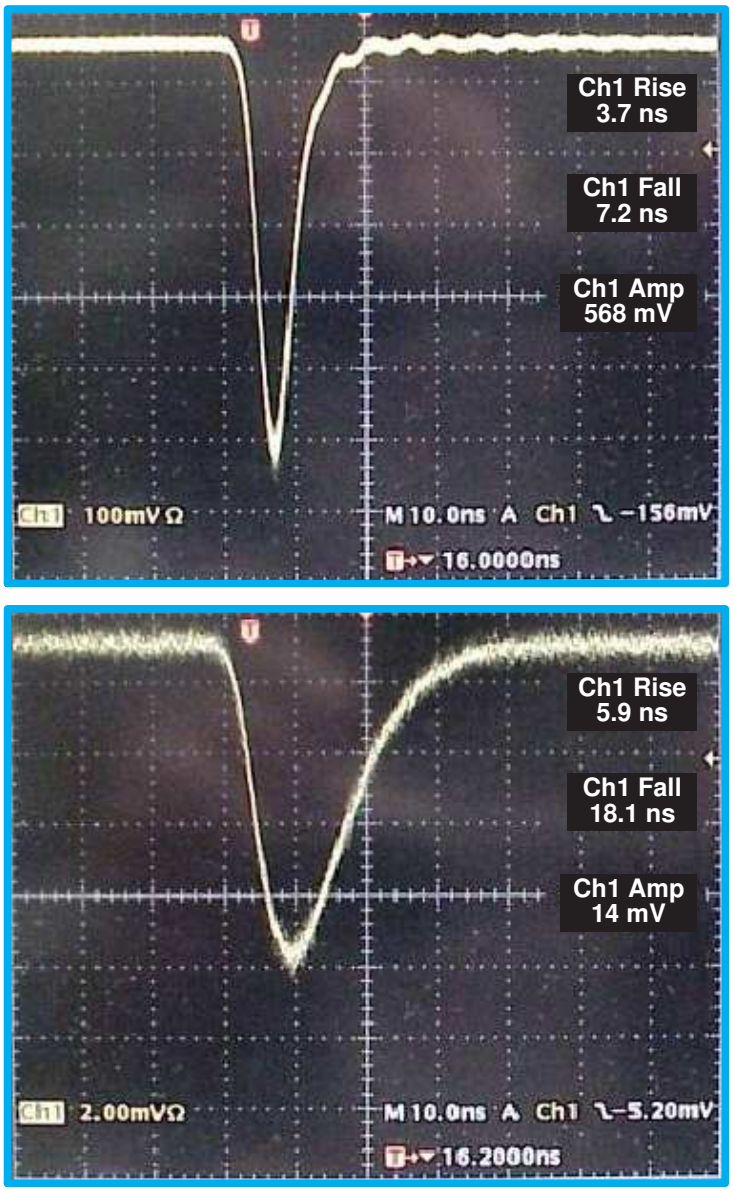

Fig. 13. PMT-9903B (left) and APD-630-70-74-510 (right) responses to short light pulses. The duration of the light pulse is about 3 ns. The intensity of the light pulse is about 40,000 photons, which corresponds to the 700-MeV photon signal.

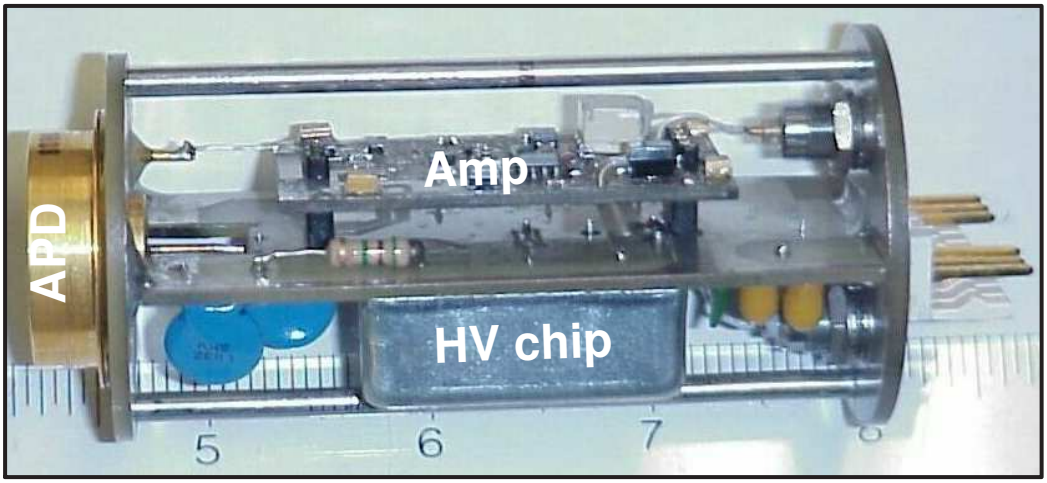

Fig. 14. View of an APD unit.

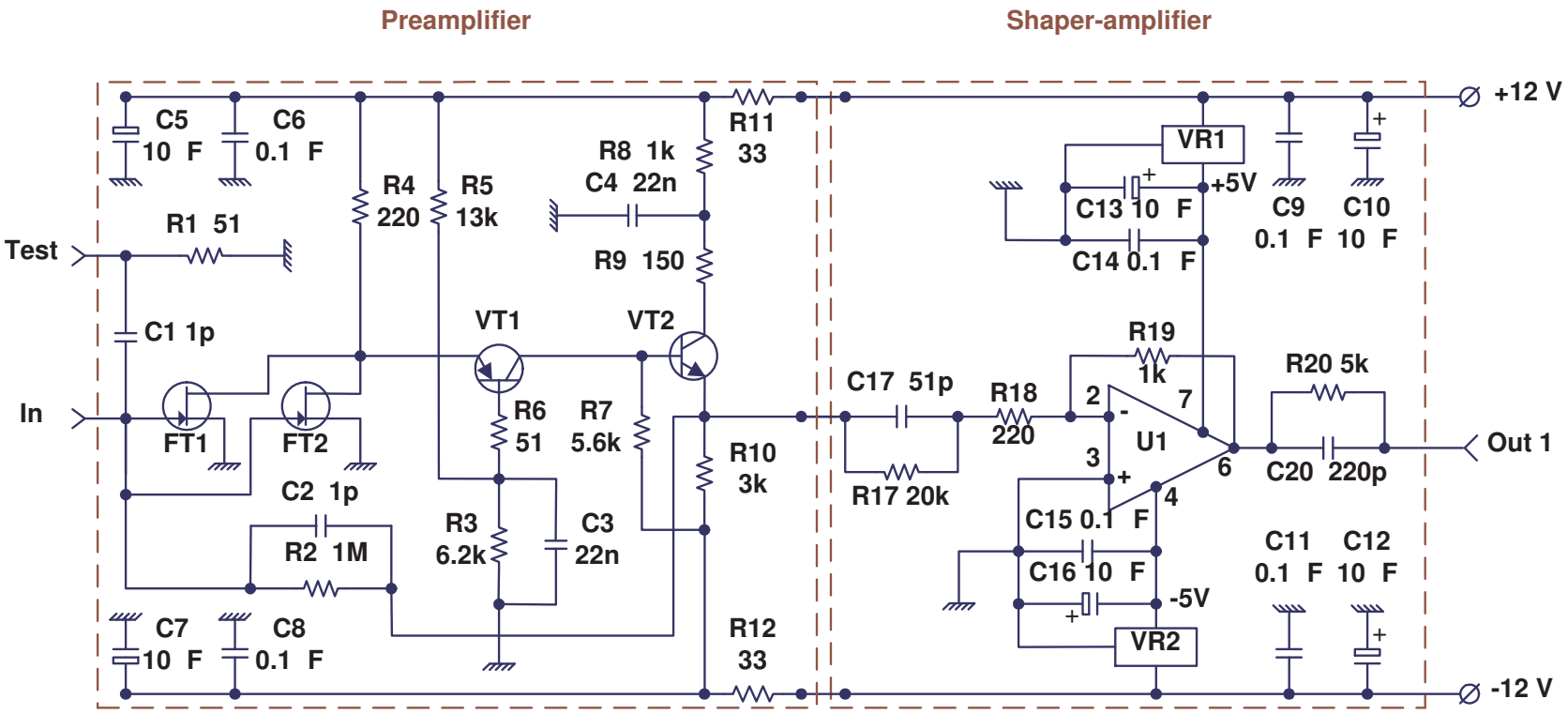

FT1 and FT2 are the 2SK2394 YJ-5 JFETs (SANYO).
VT1 is the 2N4260 bipolar transistor.
VT2 is the 2N3600 bipolar transistor.
U1 is the AD8009 amplifier (Analog Devices).
VR1 is the 78L05 Positive Voltage Regulator.
VR2 is the 79L05 Negative Voltage Regulator.
All schematic components are the surface-mount elements.

Fig. 15. The functional scheme of an APD charge sensitive amplifier.

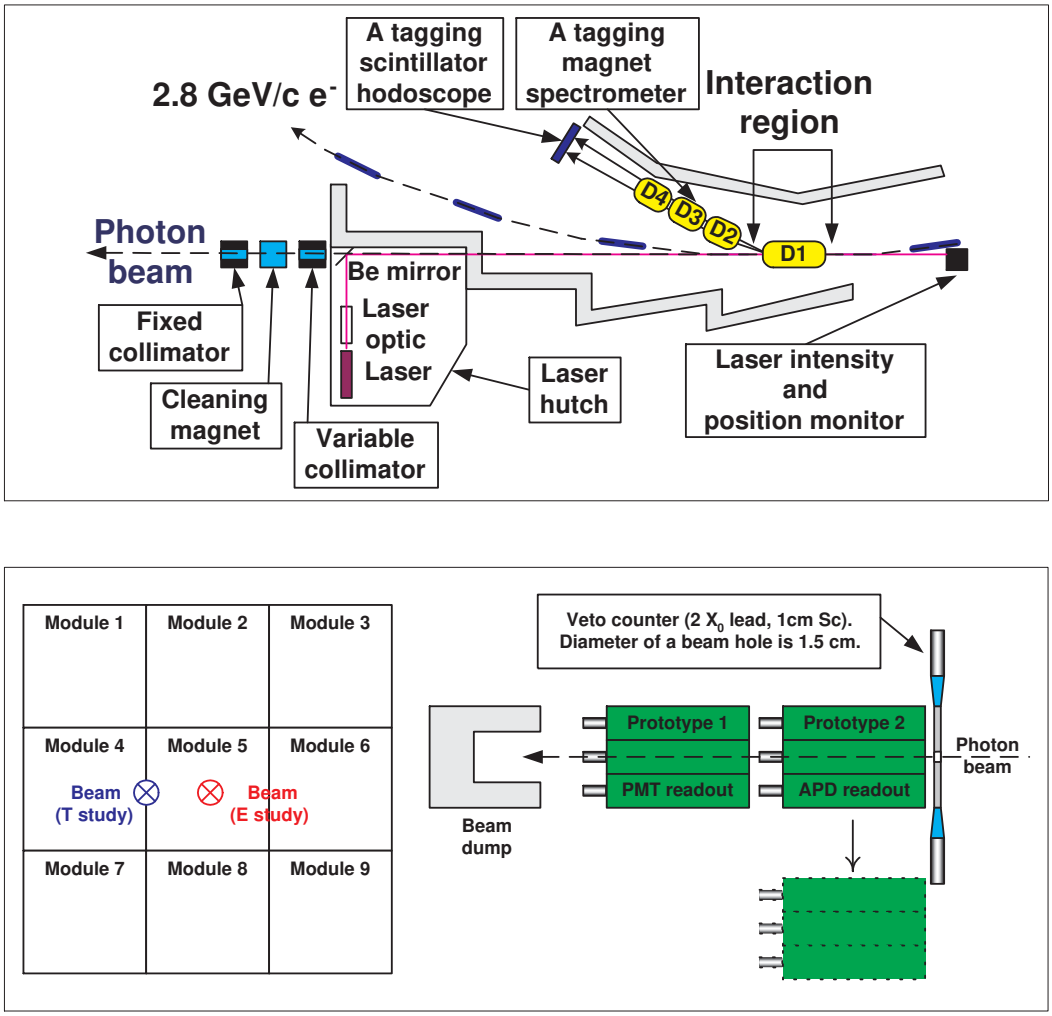

Fig. 16. The LEGS test facility floor plan. The LEGS tagged-photon beam line (X5) is shown on top. Schematic drawing of the detector setup is shown at the bottom. The left corner of the bottom picture is shows an indexing of the nonet modules and a beam position at a studied nonet for the energy, inefficiency, and timing measurements. A **E-study** mark shows the beam position during of the energy and inefficiency measurements, a **T-study** mark is the beam position during of the timing measurement.

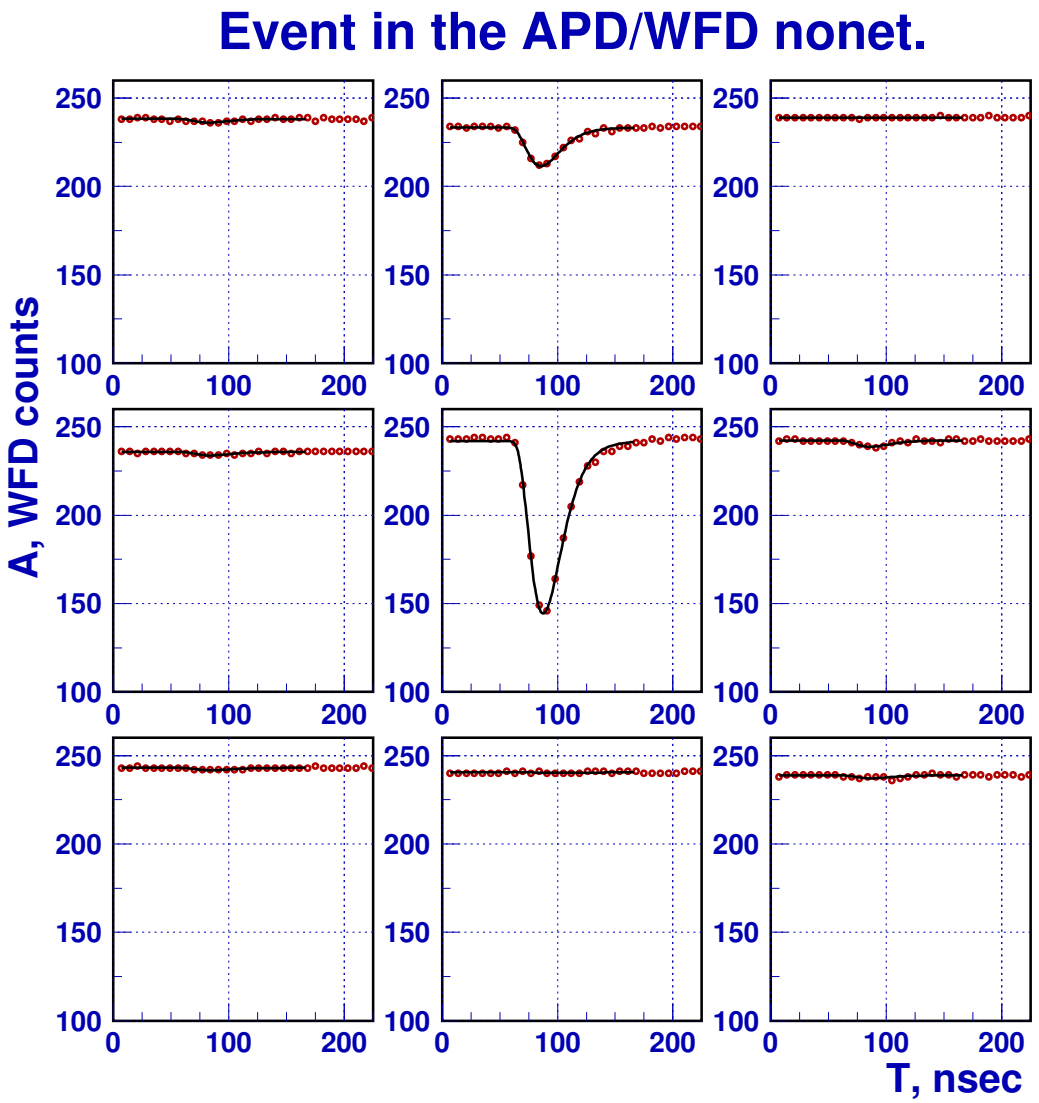

Fig. 17. A typical response of the nonet of Shashlyk modules to 340-MeV photons.

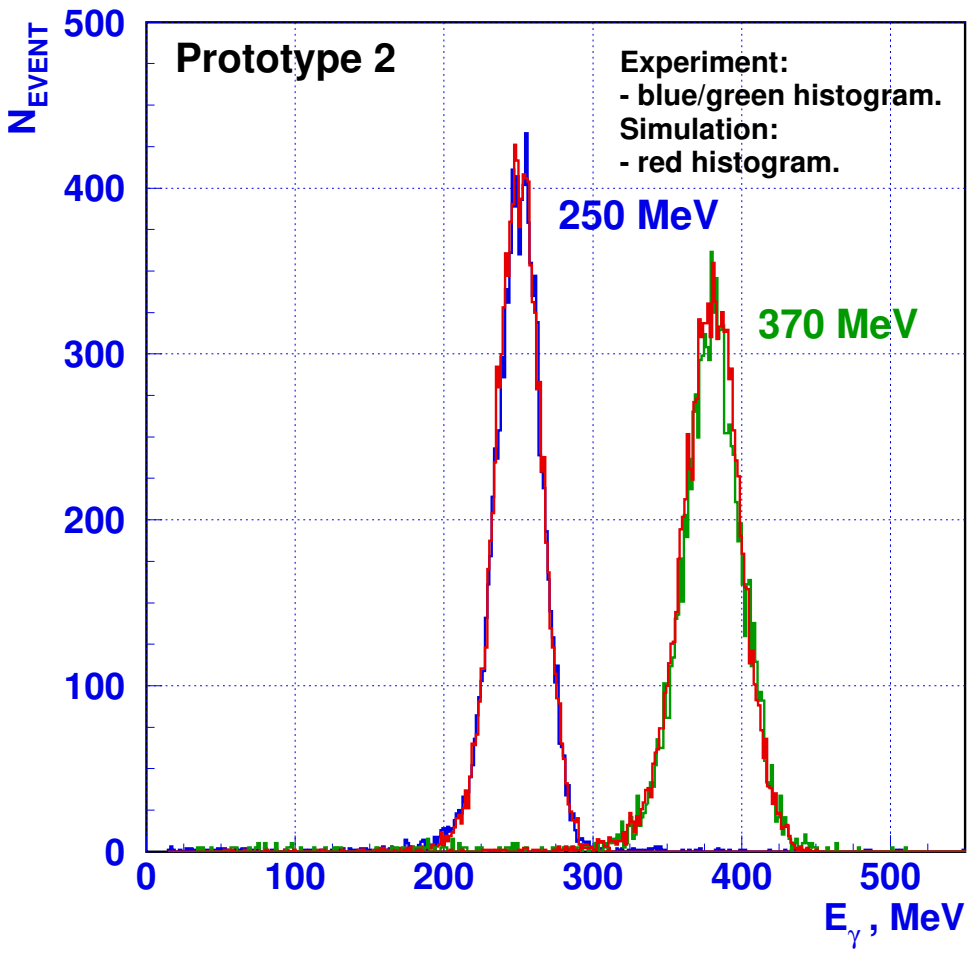

Fig. 18. Comparison of the experimental (green and blue lines) and simulated (red lines) energy spectra in the Shashlyk nonet with the APD+WFD readout.

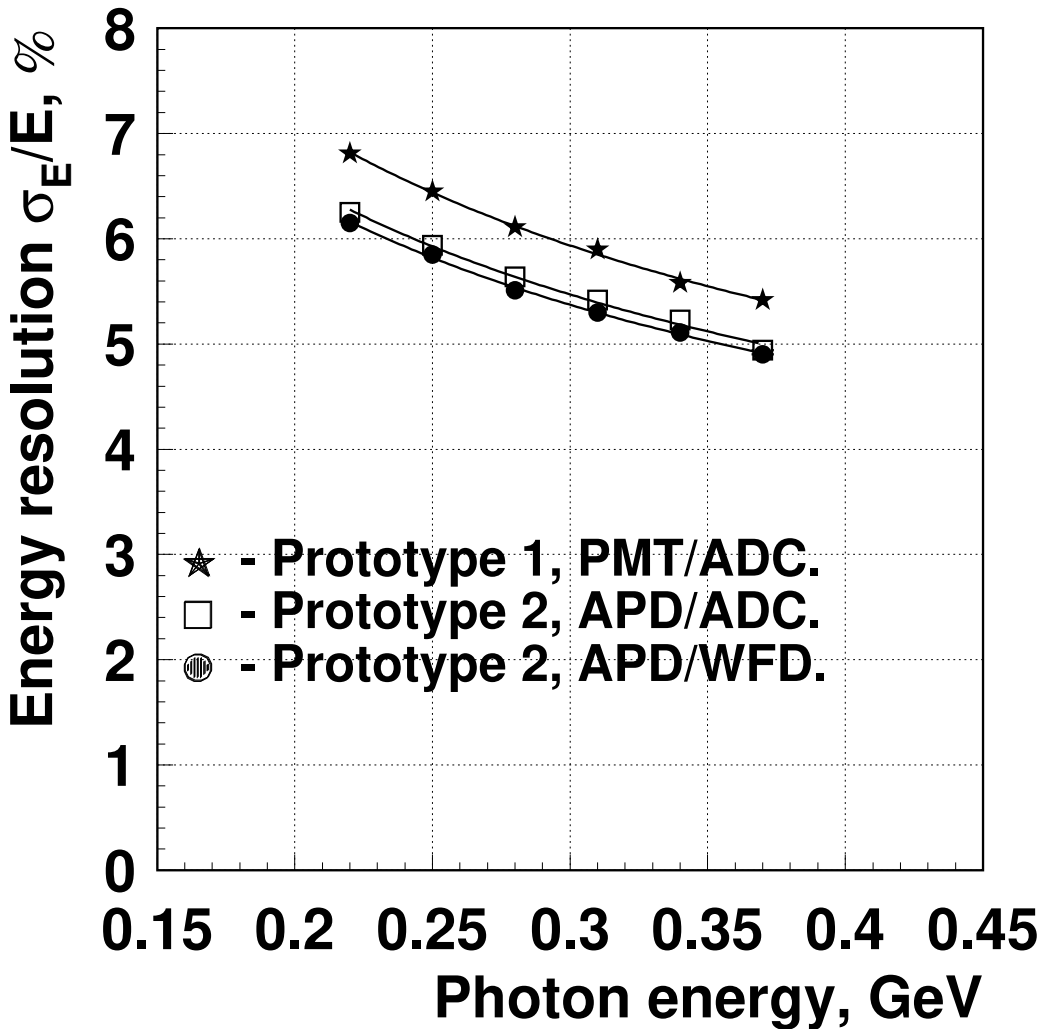

Fig. 19. Energy resolution of a prototype of the Shashlyk Calorimeter for KOPIO.

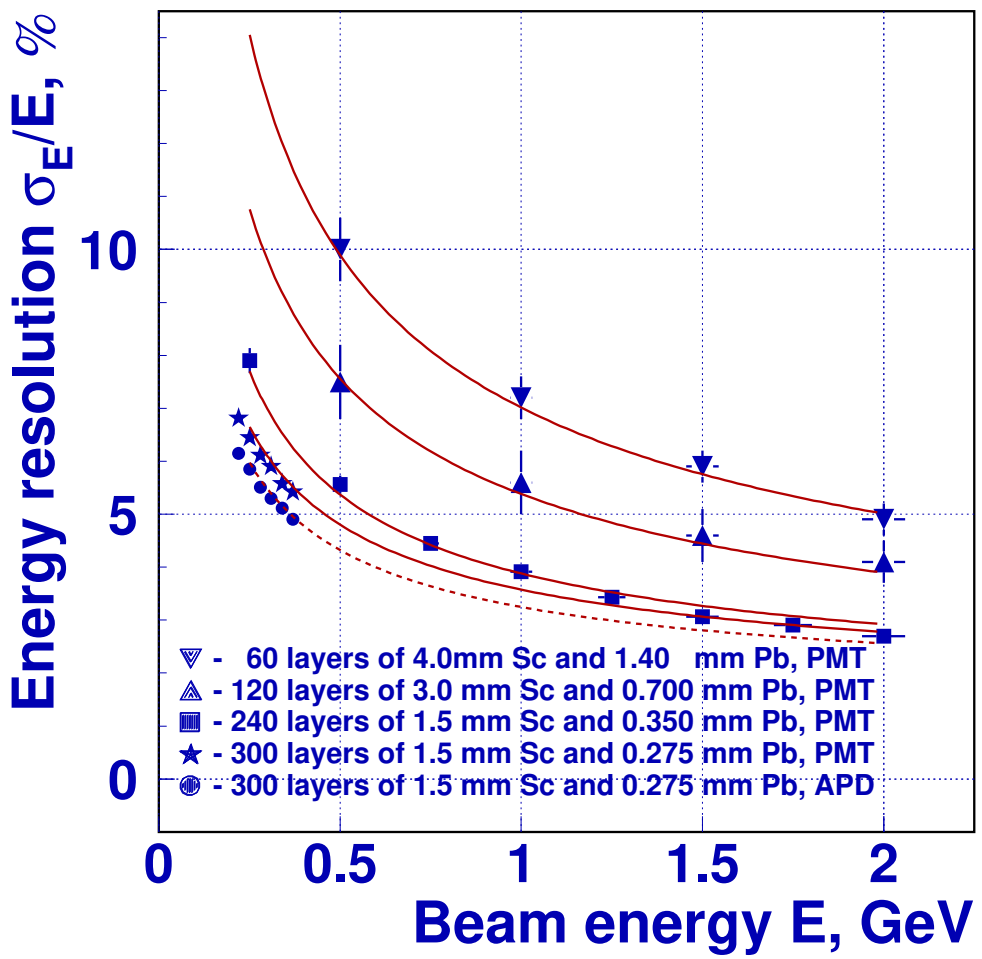

Fig. 20. The energy resolution of nonets of modules versus the energy of the electron/photon beam for configurations described in the figure. The lines show the results of simulation.

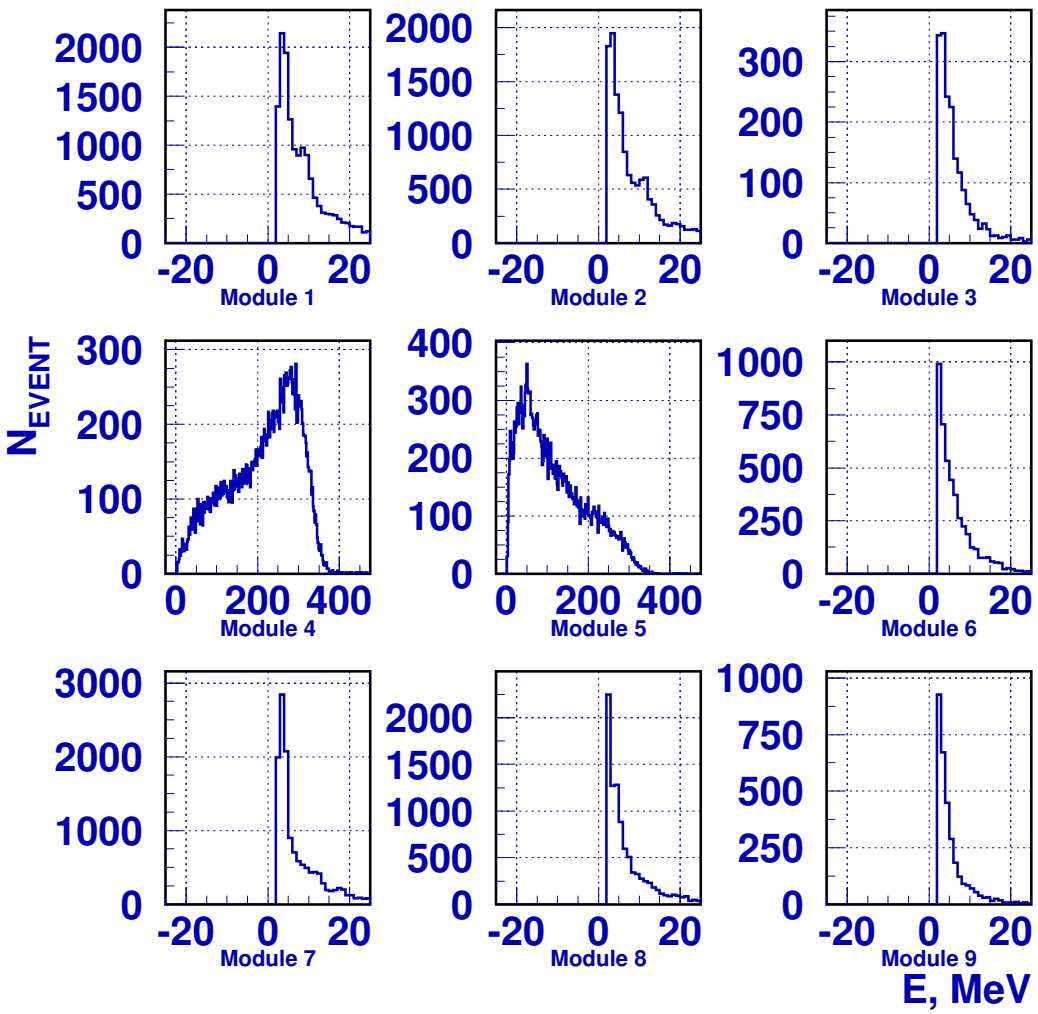

Fig. 21. The typical distribution of photon energy in the nonet of the Shashlyk modules during timing measurements. Here, 340-MeV photons hit the nonet at a boundary between central (#5) and left (#4) modules.

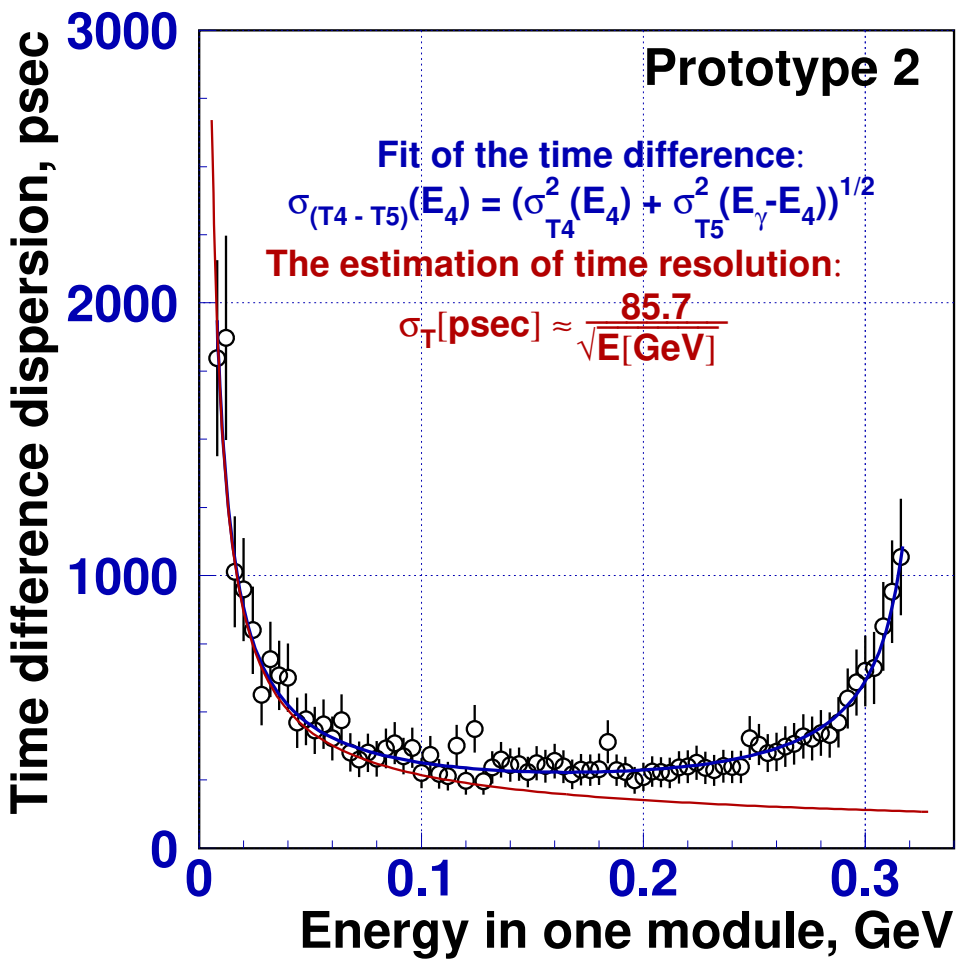

Fig. 22. Experimental evaluation of the time resolution of a Shashlyk module. Blue solid line is fit of the time difference of $\sigma_{(T4-T5)}(E_4) = \sqrt{\sigma^2_{T4}(E4) + \sigma^2_{T5}(E_\gamma - E4)}$. Red solid line is a fit-estimated time resolution of $\sigma_T \approx 90(\text{psec})/\sqrt{E_\gamma(\text{GeV})}$ in both modules.

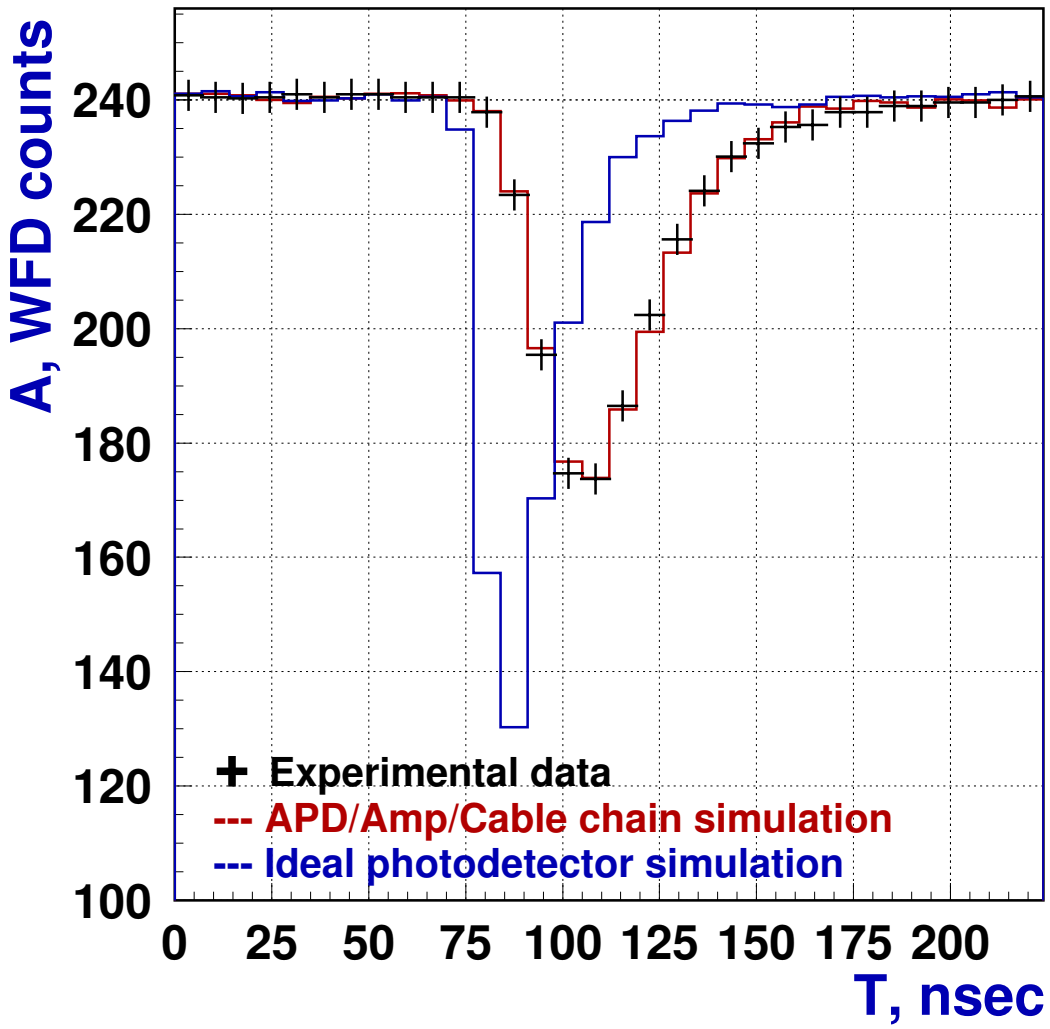

Fig. 23. The simulation of the light response function of the Shashlyk module at the entrance of the photodetector for a 250 MeV photon. The simulated signal in a Wave Form Digitizer if APD/Amplifier/Cable time-response function is taken into account is shown by dashed line.

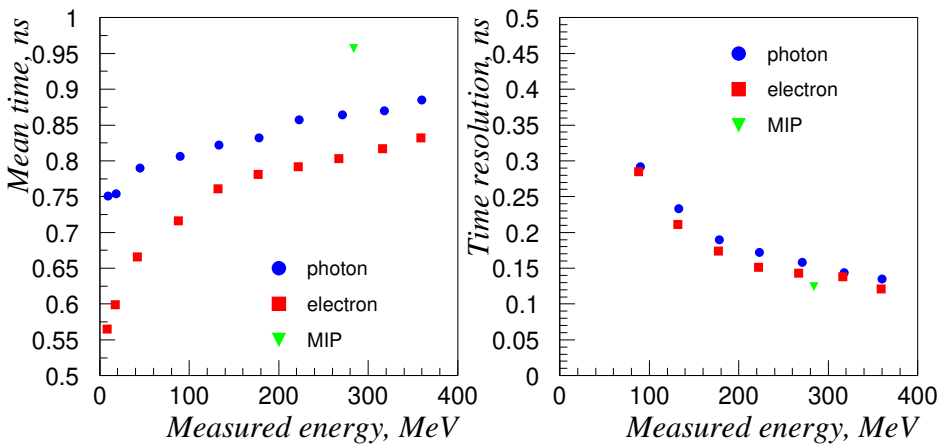

Fig. 24. Results of a Monte Carlo simulations of the time resolution of the Shashlyk module for photons, electrons, and Minimum Ionizing Particles (MIP). The solid line corresponds to a (90 ps)/$\sqrt{E\ (\mathrm{GeV})}$ time resolution, which fits our experimental photon test-beam data.

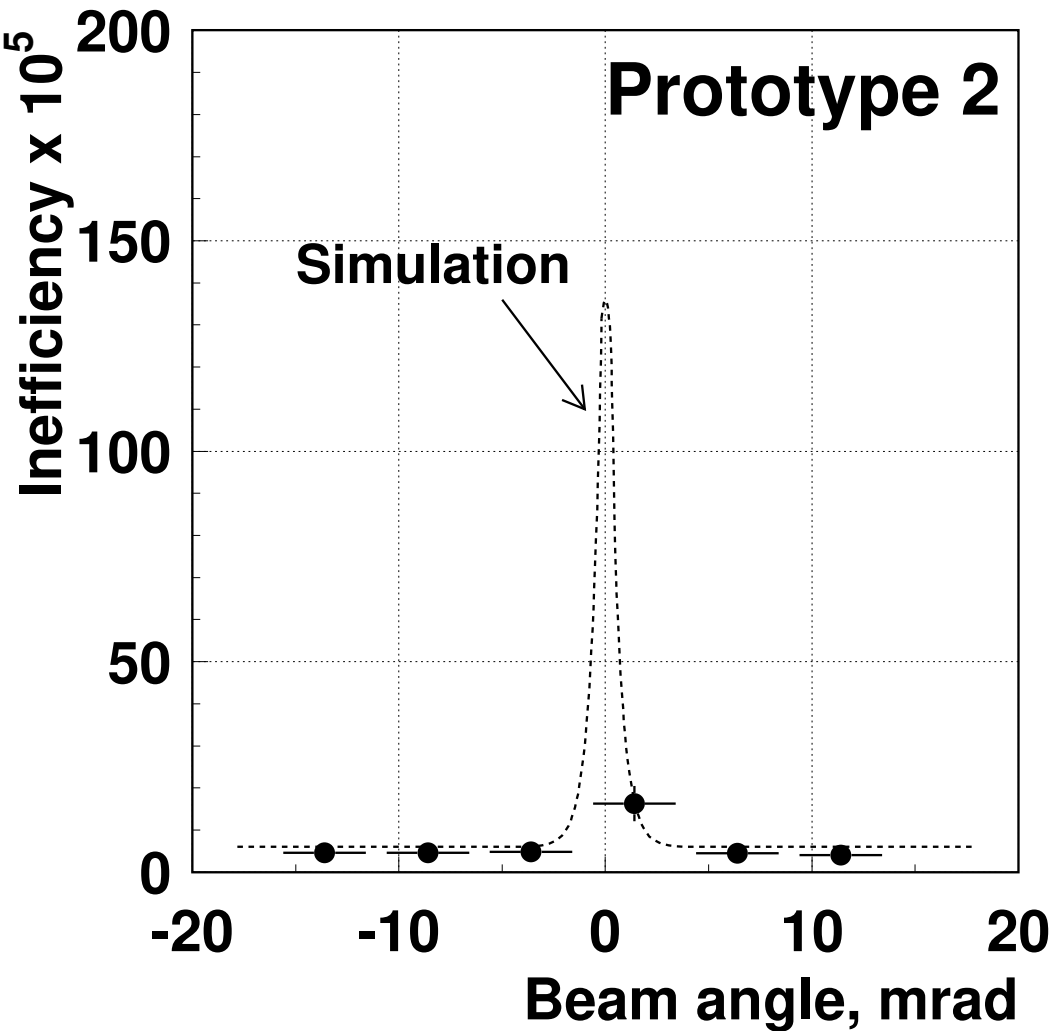

Fig. 25. The dependence of the photon detection inefficiency on the incident angle.

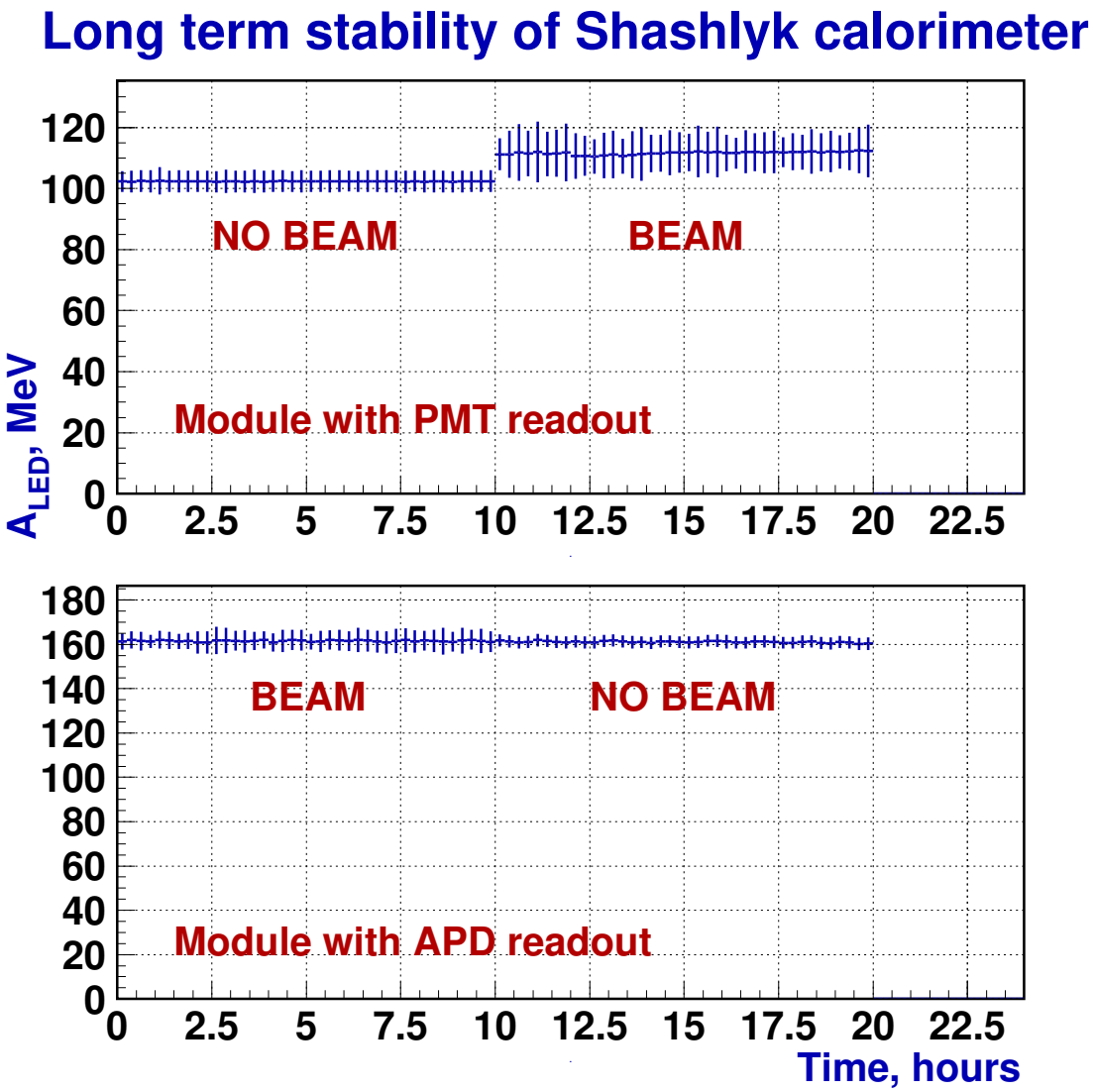

Fig. 26. Illustration of the long-term stability and gain dependence on the rate for the APD and PMT readout of the Calorimeter prototypes. The beam intensity was 300 kHz. The upper picture shows clearly the rate effect for a PMT-9903B after changing the photon beam intensity from 0 kHz to 300 kHz.